Colloquium: The unexpected properties of alkali metal iron selenide superconductors

Elbio Dagotto

Department of Physics and Astronomy, University of Tennessee, Knoxville, Tennessee 37996, USA and Materials Science and Technology Division, Oak Ridge National Laboratory, Oak Ridge, Tennessee 37831, USA

(published 20 May 2013)

The iron-based superconductors that contain FeAs layers as the fundamental building block in the crystal structures have been rationalized in the past using ideas based on the Fermi surface nesting of hole and electron pockets when in the presence of weak Hubbard U interactions. This approach seemed appropriate considering the small values of the magnetic moments in the parent compounds and the clear evidence based on photoemission experiments of the required electron and hole pockets. However, recent results in the context of alkali metal iron selenides, with generic chemical composition $A_xFe_{2-y}Se_2$ (A = alkali metal element), have challenged those previous ideas since at particular compositions y the low-temperature ground states are insulating and display antiferromagnetic order with large iron magnetic moments. Moreover, angle-resolved photoemission studies have revealed the absence of hole pockets at the Fermi level in these materials. The present status of this exciting area of research, with the potential to alter conceptually our understanding of the iron-based superconductors, is here reviewed, covering both experimental and theoretical investigations. Other recent related developments are also briefly reviewed, such as the study of selenide two-leg ladders and the discovery of superconductivity in a single layer of FeSe. The conceptual issues considered established for the alkali metal iron selenides, as well as several issues that still require further work, are discussed.

DOI: 10.1103/RevModPhys.85.849 PACS numbers: 74.70.Xa, 74.25.−q, 74.20.−z

CONTENTS

I. INTRODUCTION

One of the most active areas of research in condensed matter physics at present is the study of the high-critical-temperature (T_c) superconductors based on iron. This field started with the seminal discovery of superconductivity at 26 K in F-doped LaFeAsO (Kamihara *et al.*, 2008). Several other superconductors with a similar structure have been synthesized since 2008 [for a review, see Johnston (2010) and Stewart (2011)]. They all have FeAs or FeSe layers, which are widely believed to be the key component of these iron-based superconductors, just as the CuO_2 layers are the crucial ingredients of the famous high-T_c cuprates (Dagotto, 1994; Scalapino, 1995). The many analogies between the iron-based superconductors and the cuprates lie not only in the quasi-two-dimensional characteristics of the active layers, but also in the proximity to magnetically ordered states which in many theoretical approaches are believed to induce superconductivity via unconventional pairing mechanisms that do not rely on phonons. However, at least for the case of the iron superconductors based on As, the parent magnetic compounds are metallic, as opposed to the Mott insulators found in the cuprates, establishing an important difference between cuprates and pnictides.

The $FeAs_4$ tetrahedron is the basic building block of the FeAs layers. Materials such as LaFeAsO belong to the "1111" family, with a record T_c of 55 K for SmFeAsO (Ren *et al.*, 2008). Subsequent efforts unveiled superconductivity also in the doped versions of "122" compounds such as $BaFe_2As_2$, "111" compounds such as LiFeAs, and others (Johnston, 2010; Paglione and Greene, 2010; Hirschfeld, Korshunov, and Mazin, 2011; Stewart, 2011; Wang and Lee, 2011).

It is important to remark that there are structurally related materials, known as the "11" family, that display equally interesting properties. A typical example is FeSe, which also superconducts, although at a lower T_c of 8 K (Hsu *et al.*, 2008). FeSe has a simpler structure than the pnictides since there are no atoms in between the FeSe layers. Locally, the iron cations are tetrahedrally coordinated to Se, as it occurs in $FeAs_4$. The critical temperature can be increased dramatically by Te substitution or even more by pressure up to 37 K (Fang *et al.*, 2008; Yeh *et al.*, 2008; Margadonna *et al.*, 2009). The normal state of Fe(Se,Te) is electronically more correlated than that of iron pnictides (Tamai *et al.*, 2010). The study of iron superconductors based on Se (the iron selenides) is less advanced than similar studies in the case of As (the iron pnictides), and it is precisely the goal of this Colloquium to focus on the most recent developments in the area often referred to as the "alkaline iron selenides," with typically alkali metal elements intercalated in between the FeSe layers. Since many results described in this review use K to intercalate, the compounds in focus here will be generically called "alkali metal iron selenides" to avoid confusion with the "alkaline earth metals" (Be, Mg, Ca, Sr, Ba, and Ra). However, one should be aware that there are exceptions, such as the use of Tl in some layered compounds, Ba in the ladders treated in Sec. VIII, and more recently other alkaline earth metals to further increase T_c as described in Sec. IX. Also the more general term chalcogenides will not be used here since our focus is exclusively on compounds with FeSe layers, not with FeTe layers. At present, the field of alkali metal iron selenides is receiving considerable attention not only because the T_cs are now comparable to those of the iron pnictides but also because some of these selenides are magnetic insulators, potentially bringing closer together the fields of the iron- and copper-based superconductors.

One of the motivations for the use of alkali elements to separate the FeSe layers is that the T_c of the iron-based superconductors appears to be regulated by the "anion height," i.e., the height of the anion above the iron-square planes (Mizuguchi *et al.*, 2010; Garbarino *et al.*, 2011). Alternatively, it has been proposed that the closer $Fe(anion)_4$ is to the ideal tetrahedron, the higher T_c becomes (Qiu *et al.*, 2008). Then via chemical substitutions or intercalations T_c could be further enhanced since that process can possibly optimize the local structure.

In this Colloquium, this active field of alkali metal iron selenides will be reviewed. Before explaining the organization of this article, it is important to remark that it is not a review of the full field of iron-based superconductors, which would be a formidable task. Instead the focus is on the recent developments for compounds with chemical formulas $A_xFe_{2-y}Se_2$ (A = alkali element) that not only show superconductivity at temperatures comparable to those of the pnictides, but also present insulating and magnetic properties at several compositions, establishing a closer link to the cuprates. In fact, many studies reviewed here suggest that a proper description of $A_xFe_{2-y}Se_2$ requires an intermediate value of the Hubbard repulsion U in units of the carriers' bandwidth. This degree of electronic correlation is needed to explain, for instance, the large magnetic moment per iron atom observed in these novel compounds. Last but not least, the notorious absence of Fermi surface (FS) hole pockets in these materials, as also reviewed here, prevents the applicability of the ideas widely discussed for the iron pnictides that rely on the FS nesting between electron and hole pockets. Since there are no hole pockets, an alternative starting point is needed. It is fair to say that pnictides and selenides may be in different classes of magnetic and superconducting materials, even if the pairing arises in both cases from magnetic fluctuations. For instance, the former could be based on itinerant spin density wave states, and the latter on local moments. However, mere simplicity also suggests that pnictides and selenides may share a unique mechanism to generate their magnetic and superconducting states. If this is the case, then learning about the physics of the $A_xFe_{2-y}Se_2$ compounds may fundamentally alter the conceptual framework used for the entire field of research centered on the iron-based superconductors.

The organization of this Colloquium is as follows. In Sec. II, the early history of the alkali metal iron selenides is provided, including the ordered states of the iron vacancies. Section III addresses the existence of phase separation into superconducting and magnetic regions, and also the much debated issue of which states should be considered the parent states for superconductivity. Results obtained using a variety of experimental techniques are discussed in Sec. IV. In Sec. V, investigations using angle-resolved photoemission are reviewed, with emphasis on the two most important results: absence of hole pockets at the FS and isotropic superconducting gaps. Section VI contains the neutron scattering results, showing the exotic magnetic states in the presence of iron vacancies, particularly the block antiferromagnetic state. Theoretical calculations, using both first-principles and model Hamiltonian approaches, are given in Sec. VII. The experimentally observed phases, as well as a variety of competing states, are discussed from the theory perspective. Section VIII describes recent efforts focused on two-leg ladder selenides, which display several common aspects with the layered iron selenides. Finally, in Sec. IX several closely related topics are discussed, including the discovery of superconductivity in a single layer of FeSe. Because of length constraints some topics that would make this review self-contained, such as the crystallography of the materials of focus here, cannot be included. However, recent reviews (Johnston, 2010; Stewart, 2011) can be consulted to compensate for this missing information. A recent brief review about the alkali metal iron selenides (Mou, Zhao, and Zhou, 2011) can also be consulted for a broader perspective on this topic.

II. EARLY DEVELOPMENTS

The report that started the field of alkali metal iron selenides was published by Guo *et al.* (2010). In this publication,

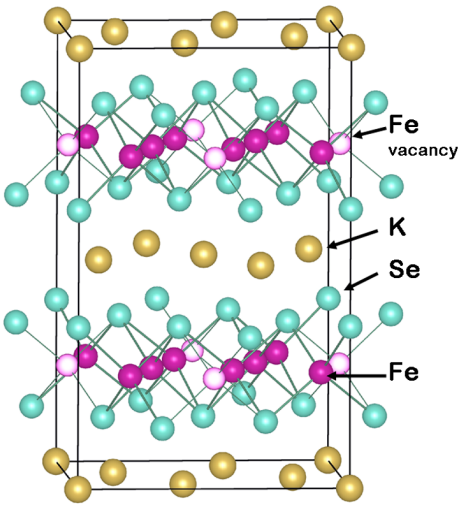

FIG. 1 (color online). Crystal structure of $A\mathrm{Fe}_x\mathrm{Se}_2$. All the other compounds described here have a similar structure. A is an alkali metal element (K in the figure). If $x < 2$, iron vacancies are present. From Bao *et al.*, 2013.

results were presented for polycrystalline samples of $\mathrm{K}_{0.8}\mathrm{Fe}_2\mathrm{Se}_2$ (nominal composition).

The crystal structure is shown in Fig. 1. It contains layers of an alkali metal element, such as K, separating the FeSe layers. As in the 122 pnictide structures based on, e.g., Ba, the FeSe layers are the "conducting layers" while the K^+ ions provide charge carriers. The K layers increase the distance between the FeSe layers, magnifying the reduced dimensionality characteristics of the material.

The resistance versus temperature is shown in Fig. 2. Upon cooling, insulating behavior is observed first (a resistance that grows with decreasing temperature), followed by a broad peak at 105 K where a metalliclike region starts. At ~30 K, the resistance abruptly drops to zero, leading to a superconducting

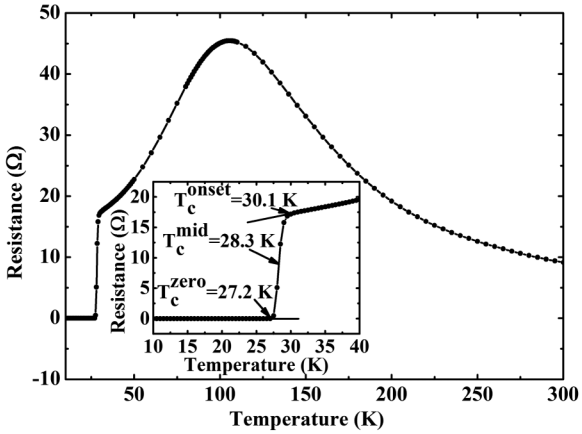

FIG. 2. Temperature dependence of the electrical resistance of polycrystalline $\mathrm{K}_{0.8}\mathrm{Fe}_2\mathrm{Se}_2$. The dominant features include the SC transition temperature at ~30 K, with the inset containing better-resolution details of that transition. The peak slightly above 100 K, later found using single crystals at higher temperatures (Mizuguchi *et al.*, 2011), is caused by the iron-vacancy ordering (D. M. Wang *et al.*, 2011). The coexistence of features related to iron vacancies and superconductivity was later explained based on phase separation (see Sec. III). From Guo *et al.*, 2010.

(SC) state. To explain the high value of the critical temperature as compared to the T_c of FeSe (8 K) or Te-doped FeSe (15.2 K), Guo *et al.* (2010) argued that the Se-Fe-Se bond angle is close to the ideal FeSe_4 tetrahedral shape and also the interlayer distance is large compared to that of FeSe.

Subsequent work employing single crystals reported that the broad resistivity peak of $\mathrm{K}_{0.8}\mathrm{Fe}_2\mathrm{Se}_2$ is actually located above 200 K, i.e., at a higher temperature than in polycrystals, and its SC critical temperature is 33 K (Mizuguchi *et al.*, 2011). Related efforts showed that the hump in the normal-state resistivity was related to the iron-vacancy ordering process (D. M. Wang *et al.*, 2011) that was shown to exist in parts of the sample, as discussed in Sec. III devoted to phase separation (i.e., some of the early samples were later shown to contain two phases, at either the nanoscopic or the microscopic length-scale levels). There was no correlation between the hump and the SC critical temperatures.

Similar properties were observed in other compounds. For instance, Krzton-Maziopa, Shermadini *et al.* (2011) reported a $T_c = 27$ K for $\mathrm{Cs}_{0.8}(\mathrm{FeSe}_{0.98})_2$. Superconductivity at $T_c = 32$ K was also found in $\mathrm{Rb}_{0.88}\mathrm{Fe}_{1.81}\mathrm{Se}_2$ (A. F. Wang *et al.*, 2011). Other studies using K and Cs as alkali elements were reported by Ying *et al.* (2011), superconductivity at 32 K was reported for (Tl, Rb)$\mathrm{Fe}_x\mathrm{Se}_2$ by Hangdong Wang *et al.* (2011), and using a mixture (Tl,K) by M. H. Fang *et al.* (2011). The latter also contains an interesting phase diagram varying the amount of iron in (Tl, K)$\mathrm{Fe}_x\mathrm{Se}_2$, constructed from the temperature dependence of the resistivity. This phase diagram displays the evolution from insulating to SC phases in the (Tl, K)$\mathrm{Fe}_x\mathrm{Se}_2$ system, resembling results in the cuprates. From anomalies in magnetic susceptibilities, several of these efforts also reported the presence of antiferromagnetic (AFM) order in regimes that are insulating at all temperatures (M. H. Fang *et al.*, 2011; Bao *et al.*, 2013). Based on previous literature on materials such as $\mathrm{TlFe}_x\mathrm{S}_2$, M. H. Fang *et al.* (2011) concluded that there must be regularly arranged iron vacancies when Se replaces S, and also a concomitant AFM order. The expected iron-vacancy order is shown schematically in Fig. 3 for the cases of $x = 1.5$, 1.6, and 2.0 in the chemical formula (Tl, K)$\mathrm{Fe}_x\mathrm{Se}_2$ (M. H. Fang *et al.*, 2011). In this context, Bao *et al.* (2013) argued that decorating the lattice

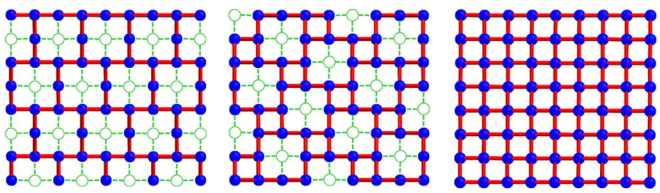

FIG. 3 (color online). (Left panel) Iron-vacancy order corresponding to $A\mathrm{Fe}_{1.5}\mathrm{Se}_2$. The solid circles are iron atoms. The open circles are vacancies. Each iron atom has either two or three iron neighbors. This type of order is called the 2×4 iron-vacancy order since along the horizontal (vertical) axis the vacancies are separated by 2 (4) Fe-Fe lattice spacings. (Center panel) The case of $A\mathrm{Fe}_{1.6}\mathrm{Se}_2$ with its $\sqrt{5} \times \sqrt{5}$ iron-vacancy distribution. All iron atoms have three iron neighbors. The label refers to the distance between nearest-neighbor vacancies which is $\sqrt{5}$ in two perpendicular directions, in units of the Fe-Fe lattice spacing. (Right panel) State with no iron vacancies, corresponding to $A\mathrm{Fe}_2\mathrm{Se}_2$, where A = (Tl, K), believed to be of relevance for the SC state. From M. H. Fang *et al.*, 2011.

with vacancies offers a new route to high-T_c superconductivity by modifying the FS and altering the balance between competing tendencies. Using x-ray diffraction and single crystals, the iron-vacancy arrangement sketched in the central panel of Fig. 3, i.e., the so-called $\sqrt{5} \times \sqrt{5}$ arrangement, was shown to be present in SC samples by Zavalij *et al.* (2011)) (and those samples have phase separation; see Sec. III). Transmission electron microscopy results also provided evidence of this type of vacancy order (Z. Wang *et al.*, 2011).

All these early discoveries established the field of alkali metal iron selenides, and the subsequent work reviewed here provided a microscopic perspective on the properties of these compounds.

III. TENDENCIES TO PHASE SEPARATION

Recent investigations showed that the often puzzling properties of several alkali metal iron selenides can be understood by realizing that phase separation occurs in these compounds. As happens in manganites and cuprates, in the materials reviewed here several length scales are involved in the phase coexistence. The two competing (or maybe cooperating) states are the SC and magnetic states, the latter with ordered iron vacancies. The coexistence of free-of-vacancies magnetism and superconductivity was also reported in pnictides (Julien *et al.*, 2009; Johnston, 2010). Next a summary of results on phase separation in selenides is presented, ordered by technique but also approximately chronologically.

A. Muon-spin rotation

The microscopic coexistence of magnetism and superconductivity was reported via muon-spin spectroscopy investigations of $Cs_{0.8}(FeSe_{0.98})_2$ (Shermadini *et al.*, 2011) and $A_xFe_{2-y}Se_2$ (A = Rb, K) (Shermadini *et al.*, 2012). Additional evidence for phase separation was provided by simultaneous angle-resolved photoemission spectroscopy (ARPES) and muon-spin rotation (μSR) analysis of $Rb_{0.77}Fe_{1.61}Se_2$ with $T_c = 32.6$ K (Borisenko *et al.*, 2012). This study showed that the results can be rationalized via a macroscopic separation into metallic ($\sim 12\%$) and insulating ($\sim 88\%$) phases. The metallic component appears associated with $RbFe_2Se_2$, and Borisenko *et al.* (2012) believed that the insulating component is a competing order, not relevant for superconductivity. Instead, they argued that van Hove singularities are the key ingredient for superconductivity. On the other hand, studies of the resistivity and magnetic susceptibility of $A_{0.8}Fe_{2-y}Se_2$ are also interpreted as coexisting superconductivity and antiferromagnetism (Liu *et al.*, 2011) but not simply competing with each other. While phase separation between magnetic and SC states is experimentally proven, the implications are still under debate. If antiferromagnetism and superconductivity coexist microscopically, or at least are so close in space that they can influence one another, does AFM induce or suppress SC?

B. Raman scattering, transmission electron miscroscopy, and x rays

Phase separation with mutual exclusion between insulating and SC states, at the micrometer scale, was also proposed from the analysis of Raman scattering experiments on $A_{0.8}Fe_{1.6}Se_2$, where the intensity of a two-magnon peak decreases sharply upon entering the SC phase (Zhang, Liu *et al.*, 2012; Zhang, Xiao *et al.*, 2012). Transmission electron microscopy (TEM) on $K_{0.8}Fe_xSe_2$ and KFe_xSe_2 by Z. Wang *et al.* (2011) also provided evidence of nanoscale phase separation (i.e., not a coexistence of the two states but physical separation), including the formation of stripe patterns at the micrometer scale together with nanoscale phase coexistence between magnetic and SC phases (Z. W. Wang *et al.*, 2012). Percolative scenarios involving weakly coupled SC islands were also discussed by Shen *et al.* (2011) and Z. W. Wang *et al.* (2012).

X-ray absorption and emission spectroscopy applied to $K_{0.8}Fe_{1.6}Se_2$ also reported coexisting electronic phases and found superconductivity to have glassy (granular) characteristics (Simonelli *et al.*, 2012). Using scanning nanofocus x-ray diffraction, studies of the same compound focusing down to a size of 300 nm collected thousands of diffraction patterns that allowed for the construction of a real-space imaging of the *k*space results obtained by diffraction. These results provided explicit images of the intrinsic phase separation below 520 K, and they contain an expanded lattice, compatible with a magnetic state in the presence of iron vacancies, and a compressed lattice with nonmagnetic characteristics (A. Ricci *et al.*, 2011) (see Fig. 4). Micrometer-sized regions with percolating magnetic or nonmagnetic domains form a multiscale complex network of the two phases.

Note that, for phase separation at large length scales, x-ray diffraction techniques are sufficient to observe two structurally distinct phases (Bosak *et al.*, 2011; X. G. Luo *et al.*, 2011; Lazarević *et al.*, 2012; Y. Liu *et al.*, 2012; Pomjakushin *et al.*, 2012). This shows that the SC phase is a real bulk phase rather than an interfacial property. It is for shorter length scales that more microscopic techniques are needed to clarify the interplay between the two phases.

C. ARPES and phase separation

Using ARPES and high-resolution TEM applied to $K_xFe_{2-y}Se_2$, evidence was provided for a mesoscopic phase separation at the scale of several nanometers between the SC and semiconducting phases and the AFM insulating phases (F. Chen *et al.*, 2011). One of the insulators has the $\sqrt{5} \times \sqrt{5}$ iron-vacancy pattern. A sketch of these results is shown in

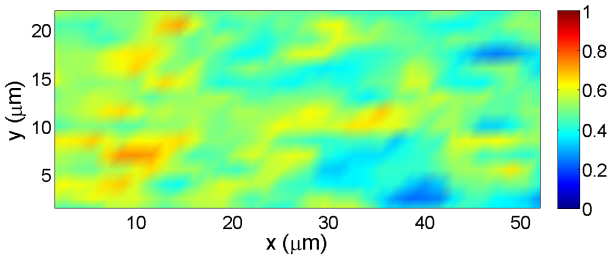

FIG. 4 (color online). Spatial distribution of the ratio of the compressed and the expanded phases in a region of size 22×55 μm^2 of a $K_{0.8}Fe_{1.6}Se_2$ crystal. Illustration of several length scales involved in the phase-separated state, resembling those found in cuprates and manganites. From A. Ricci *et al.*, 2011.

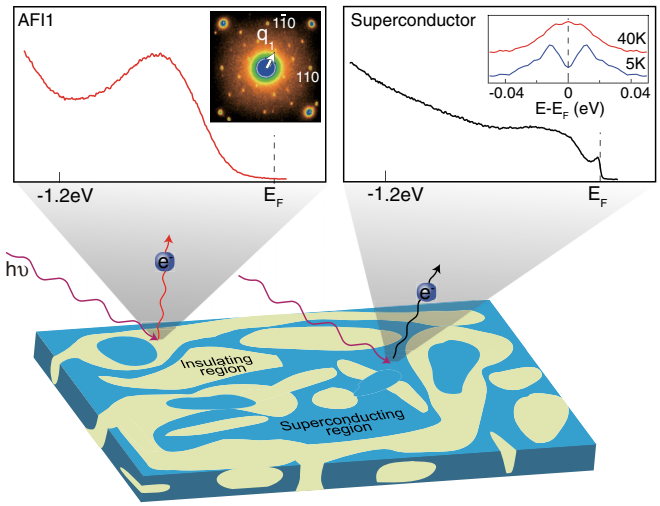

FIG. 5 (color online). Cartoon of the phase separation in superconducting $K_xFe_{2-y}Se_2$, obtained via photoemission and TEM techniques. The upper insets are the photoemission signals for the two regions: the left region corresponds to the $\sqrt{5}\times\sqrt{5}$ vacancy order, while the right region is the density of states of a superconductor. From F. Chen *et al.*, 2011.

Fig. 5. F. Chen *et al.* (2011) remarked that the insulators are mesoscopically separated from the SC or semiconducting phases, and they believe that the semiconducting phase (free of magnetic and vacancy order) is the parent compound that upon electron doping leads to superconductivity.

D. Scanning tunneling microscopy and neutron diffraction

Using thin films of $K_xFe_{2-y}Se_2$ grown using molecular-beam epitaxy techniques, scanning tunneling microscopy (STM) results were interpreted as caused by the samples containing two phases: an insulating one with the $\sqrt{5}\times\sqrt{5}$ iron vacancies and a SC state with the composition KFe_2Se_2 free of vacancies (Li *et al.*, 2012a). The densities of states (DOS) of the two phases measured via scanning tunneling spectroscopy (STS) are in Fig. 6. It is interesting that the SC phase is associated with the 122 rather than the 245 composition that contains the ordered iron vacancies, which naively was expected to be the parent compound.

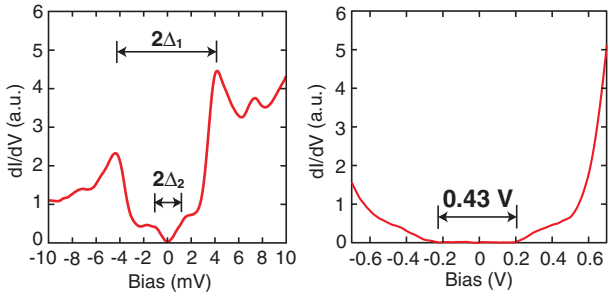

FIG. 6 (color online). (Left panel) STS results showing the DOS of a region of a $K_xFe_{2-y}Se_2$ film that displays features compatible with a SC phase. (Right panel) As the left, but for another region of the film, with results this time compatible with an insulating phase, presumably with ordered iron vacancies. From Li *et al.*, 2012a.

In related STS studies of $K_{0.73}Fe_{1.67}Se_2$ by Cai *et al.* (2012), a SC gap was found microscopically coexisting with a so-called $\sqrt{2}\times\sqrt{2}$ charge-density modulation. The iron-vacancy order was actually not observed, and Cai *et al.* (2012) argued that it is not a necessary ingredient for superconductivity. In fact, their results in the region of the charge modulation are compatible with a ferromagnetic block state in the absence of the $\sqrt{5}\times\sqrt{5}$ iron-vacancy order, as predicted by Li, Dong *et al.* (2012); see Fig. 17. Other STM studies of $K_xFe_{2-y}Se_{2-z}$ (Li *et al.*, 2012b) concluded that KFe_2Se_2 is the parent compound of superconductivity (with this state being induced by Se vacancies or via the interaction with the nearby 245 regions perhaps by modifying the doping concentration). This STM study concluded that the phase with the $\sqrt{2}\times\sqrt{2}$ charge ordering is not superconducting, since the density-of-states dip still has a nonzero value at the minimum and the results are temperature independent from 0.4 to 4.2 K, and for superconductivity to arise a contact with the $\sqrt{5}\times\sqrt{5}$ is needed. The length scale unveiled in this effort is mesoscopic (Li *et al.*, 2012b). The 122 phase charge modulation is compatible with a block spin order without iron vacancies (Li, Dong *et al.* (2012)), since the distance between equivalent ferromagnetic blocks (with spins pointing in the same direction) is $2\sqrt{2}$ times the Fe-Fe distance. Li *et al.* (2012b) also reported an exotic $\sqrt{2}\times\sqrt{5}$ charge ordering superstructure [see Fig. S3 of Li *et al.* (2012b)].

Recently another possibility was presented. Using neutron diffraction techniques for $K_xFe_{2-y}Se_2$, Zhao *et al.* (2012) proposed the state in Fig. 3 (left panel), with a rhombus-type iron-vacancy order, as the parent compound of the SC state. In this state the iron spins have parallel (antiparallel) orientations along the direction where the iron vacancies are separated by four (two) lattice spacings. This state has ideal composition $KFe_{1.5}Se_2$, iron magnetic moments $2.8\mu_B$, and an AFM band-semiconductor character, as in the first-principles calculations by Yan *et al.* (2011b). FS nesting is not applicable in this state and the large moments suggest that correlation effects cannot be neglected. The semiconducting nature of this state is also compatible with ARPES experiments (F. Chen *et al.*, 2011) that also proposed a semiconductor as the parent compound.

E. Optical spectroscopy

Optical spectroscopy studies of $K_{0.75}Fe_{1.75}Se_2$ by Yuan *et al.* (2012) revealed a sharp reflectance edge below T_c at a frequency much below the SC gap, on an incoherent electronic background. This edge was interpreted as caused by a Josephson-coupling plasmon in the SC condensate. This study provided evidence for nanoscale phase separation between superconductivity and magnetism. The coupling between the two states can be understood if it occurs at the nanometer scale, since at this scale there is a large fraction of phase boundary in the sample, while at a longer length scale a very weak coupling between the states exists (Yuan *et al.*, 2012). Infrared spectroscopy studies of $K_{0.83}Fe_{1.53}Se_2$ were also presented (Z. G. Chen *et al.*, 2011), revealing abundant phonon modes that could be explained by the iron-vacancy ordering. Studies of the complex dielectric function of $Rb_2Fe_4Se_5$ (Charnukha *et al.*, 2012b) also concluded that

there are separated SC and magnetic regions in this compound. Investigations via optical microscopy and muon-spin rotation reported an intriguing self-organization of this phase-separated state into a quasiregular heterostructure (Charnukha *et al.*, 2012a).

Other optical studies (Homes *et al.*, 2012a) initially characterized $K_{0.8}Fe_{2-y}Se_2$ as a phase-separated Josephson phase, with inhomogeneous characteristics. However, more recent studies (Homes *et al.*, 2012b) distinguished between the volume-average measurements of the original report (Homes *et al.*, 2012a) and the results arising from an effective-medium analysis (EMA) to determine which fraction of the material is actually metallic or superconducting. The volume-average case has a normal resistance too high for coherent transport, locating this case in the Josephson-coupling region, as shown in Fig. 7 which contains a scaling plot previously used to discuss cuprates and other iron-based superconductors. However, the material is not homogeneous and the EMA shows that only 10% is metallic or SC. Homes *et al.* (2012b) then concluded that if a sample could be constructed composed of just this phase, then it would be a coherent metal, falling closer to the other iron-based materials as shown also in Fig. 7. This is in agreement with the conclusions by C. N. Wang *et al.* (2012) using muon-spin rotation and infrared spectroscopy. The use of the EMA to rationalize results in phase-separated systems was also suggested by Charnukha *et al.* (2012a, 2012b).

In summary, the discussion regarding the characteristics of the parent compound of the superconducting KFe_2Se_2 state is still very fluid, defining an intriguing and exciting area of research of much importance. Several candidate states have been proposed for the parent composition of the SC state.

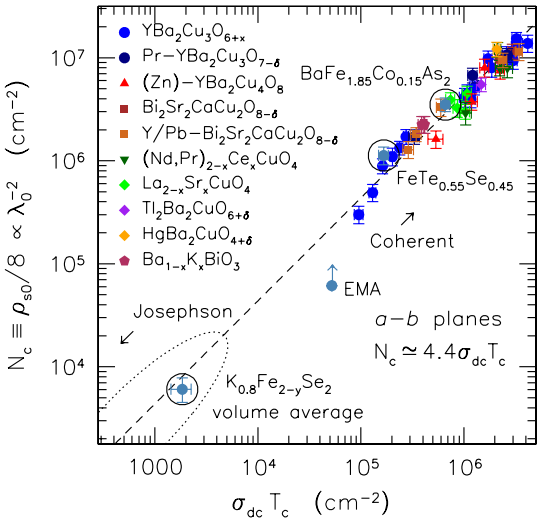

FIG. 7 (color online). Log-log plot of the spectral weight of the superfluid density N_c vs the residual conductivity σ_{dc} times the critical temperature T_c. Results include those for cuprate superconductors and several iron-based superconductors, and the volume-average and effective-medium approximation (EMA) results for $K_{0.8}Fe_{2-y}Se_2$. While the volume average signals a Josephson phase, the EMA result is now very close to the coherent regime. From Homes *et al.*, 2012b.

IV. RESULTS USING NUCLEAR MAGNETIC RESONANCE, TEM, MÖSSBAUER, AND SPECIFIC HEAT TECHNIQUES

^{77}Se nuclear magnetic resonance (NMR) studies and Knight-shift studies of $K_{0.82}Fe_{1.63}Se_2$ and $K_{0.86}Fe_{1.62}Se_2$ below T_c have demonstrated that the superconductivity is in the spin-singlet channel, although without coherence peaks in the nuclear spin-lattice relaxation rate below T_c suggesting that the state is probably nonconventional (Weiqiang Yu *et al.*, 2011). These results are similar to those known from the pnictides. Moreover, above T_c the temperature dependence of $1/T_1$ indicates that the system behaves as a Fermi liquid, suggesting the absence of strong low-energy spin fluctuations at the Se site (Weiqiang Yu *et al.*, 2011). Other ^{77}Se NMR measurements of $K_{0.65}Fe_{1.41}Se_2$ (Torchetti *et al.*, 2011) and ^{77}Se and ^{87}Rb NMR studies of $Tl_{0.47}Rb_{0.34}Fe_{1.63}Se_2$ (Ma *et al.*, 2011) arrived at similar conclusions. Torchetti *et al.* (2011) also suggested that the K vacancies may have a superstructure and the symmetry of the Se sites is lower than the tetragonal fourfold symmetry of the average structure. In addition, transmission electron microscopy experiments on $K_xFe_{2-y}Se_2$ suggested the ordering of the K ions in the a-b plane, and also addressed the resistivity hump anomaly in the iron-vacancy ordering (Li *et al.*, 2011; Song *et al.*, 2011). Using ^{77}Se NMR, the absence of strong AFM spin correlations was also reported for superconducting $K_{0.8}Fe_2Se_2$, with a nonexponential behavior in the nuclear spin-lattice relaxation rate $1/T_1$ which does not indicate a single isotropic gap (Kotegawa *et al.*, 2011, 2012). ^{77}Se and ^{87}Rb NMR studies of $Rb_{0.74}Fe_{1.6}Se_2$ also reported two coexisting phases (Texier *et al.*, 2012), and the SC regions do not have iron vacancies or magnetic order.

Mössbauer spectroscopy studies of superconducting $Rb_{0.8}Fe_{1.6}Se_2$ also report the presence of 88% magnetic and 12% nonmagnetic Fe^{2+} regions (Ksenofontov *et al.*, 2011), compatible with previously discussed reports. The magnetic properties of superconducting $K_{0.80}Fe_{1.76}Se_2$ were also studied using Mössbauer spectroscopy (Ryan *et al.*, 2011). Magnetic order involving large iron magnetic moments is observed from well below the $T_c \sim 30$ K to the Néel temperature $T_N = 532$ K.

Via the study of the low-temperature specific heat, nodeless superconductivity and strong-coupling characteristics were reported by Zeng *et al.* (2011) for single crystals of $K_xFe_{2-y}Se_2$, compatible with results found using ARPES techniques. On the other hand, thermal transport results for superconducting $K_{0.65}Fe_{1.41}Se_2$ were interpreted as corresponding to a weakly or intermediately correlated superconductor by Wang, Lei, and Petrovic (2011a, 2011b). A numerical study of the thermal conductivity and specific heat angle-resolved oscillations in a magnetic field for $A_yFe_2Se_2$ superconductors addressed the gap structure and presence of nodes (Das *et al.*, 2012), concluding that care must be taken in the interpretation of results using these techniques since even for isotropic pairing over an anisotropic FS, thermodynamic quantities can exhibit oscillatory behavior.

V. ARPES

Several photoemission experiments have been carried out for the alkali metal iron selenides. Their common result is the

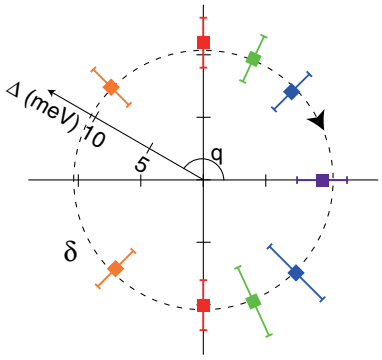

FIG. 8 (color online). Magnitude of the SC gap of $K_{0.8}Fe_2Se_2$ corresponding to the *M* point electron pockets (there are no hole pockets in this compound). The radius represents the gap while the polar angle θ is measured with respect to the M-Γ direction defined as $\theta = 0$. The results indicate that there are no nodes and also that the gap is fairly uniform, i.e., not strongly momentum dependent. Here the $M = (\pi, \pi)$ point is 45° rotated with respect to the Fe-Fe axes with regard to unit cells. In the iron-sublattice convention, this point would be $(\pi, 0)$ or $(0, \pi)$. From Y. Zhang *et al.*, 2011.

absence of hole pockets at the FS in materials that are nevertheless still SC. For instance, ARPES studies of $A_xFe_2Se_2$ (A = K, Cs; nominal composition) by Y. Zhang *et al.* (2011) revealed large electronlike pockets at the zone corner FS with wave vectors $(\pi, 0)$ and $(0, \pi)$ (in the iron-sublattice notation), with an almost isotropic (i.e., nodeless) SC gap ~10.3 meV (see Fig. 8). Hole pockets were not found at the Γ point. Y. Zhang *et al.* (2011) remarked that FS nesting between hole and electron pockets is not a necessary ingredient for the superconductivity of these materials.

Similar ARPES results were presented for $K_{0.8}Fe_{1.7}Se_2$ by Qian *et al.* (2011). Their study reported the presence of electron pockets at the zone boundary, nodeless superconductivity, and a hole band at Γ with the top of the band at ~90 meV below the Fermi level (see Fig. 9). Qian *et al.* (2011) remarked that if the FS nesting theories are used, then nesting between the electron pockets with wave vector (π, π) should dominate (as explained in the theoretical efforts summarized in Sec. VII), contrary to what appears to occur in other iron-based superconductors. Note also that FS nesting between electronlike and holelike pockets is required for

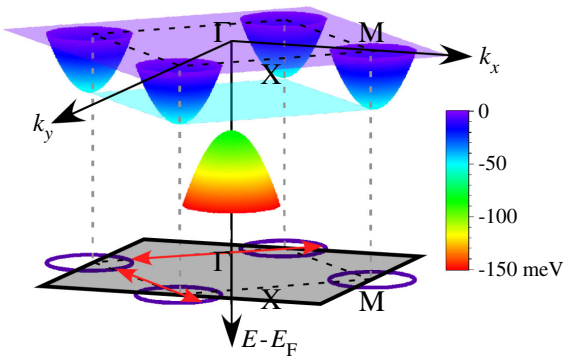

FIG. 9 (color online). Schematic diagram summarizing the electronic band structure of $K_{0.8}Fe_{1.7}Se_2$ obtained from ARPES, with the top of the hole band at the Γ point located below the FS. From Qian *et al.*, 2011.

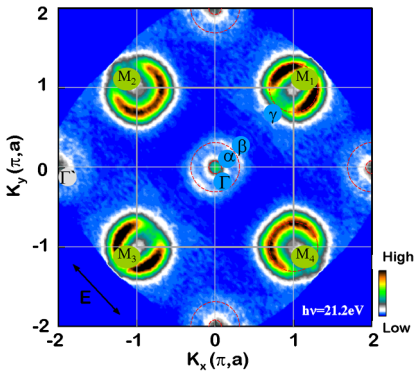

FIG. 10 (color online). FS of $(Tl_{0.58}Rb_{0.42})Fe_{1.72}Se_2$, from ARPES studies (Mou *et al.*, 2011). Note the presence of a small Γ pocket that has electronlike energy dispersion. The lattice constant a is 3.896 Å. The M points are equivalent to the $(\pi, 0)$ and $(0, \pi)$ points in the iron-sublattice notation.

the magnetic susceptibility to be enhanced, and nesting involving only electron pockets may not be sufficient to address the magnetic states. The same group also studied $Tl_{0.63}K_{0.37}Fe_{1.78}Se_2$ arriving at similar conclusions with regard to the electron pockets at $(\pi, 0)$ and $(0, \pi)$ (iron-sublattice convention), but in addition they also observed an unexpected electronlike pocket at Γ. This electron pocket has a SC gap of value comparable to that at the zone boundary pockets (X.-P. Wang *et al.*, 2011).

Studies of $(Tl_{0.58}Rb_{0.42})Fe_{1.72}Se_2$ using ARPES also led to similar conclusions (Mou *et al.*, 2011), including the presence of small electronlike FS sheets around the Γ point (see Fig. 10) and a nearly isotropic SC gap of value ~12 meV at the M points. While the SC gap at the larger Γ-point sheet is also nearly isotropic, for the inner small Γ-sheet pocket there is no SC gap. The same group also reported ARPES studies for $K_{0.68}Fe_{1.79}Se_2$ (T_c = 32 K) and $(Tl_{0.45}K_{0.34})Fe_{1.84}Se_2$ (T_c = 28 K) (Lin Zhao *et al.*, 2011). These results establish a universal FS topology and SC gap in the $A_xFe_{2-y}Se_2$ materials: there are no FS holelike pockets at Γ (thus there is no FS nesting as in some pnictides) and the SC gaps at the FS electron pockets are isotropic (nodeless).

Recent ARPES studies of $K_xFe_{2-y}Se_2$ focused on the SC gap of the small electron Fermi pocket around the Z point. An isotropic SC gap ~8 meV was reported in that pocket (see Fig. 11), and Xu *et al.* (2012) concluded that the symmetry of the order parameter must be s wave since a d wave should

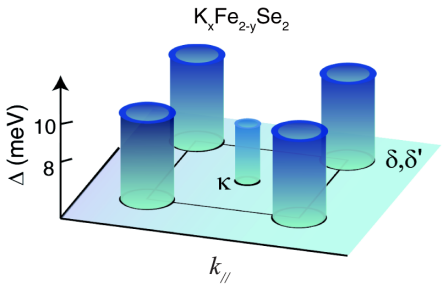

FIG. 11 (color online). Sketch of the SC gap of $K_xFe_{2-y}Se_{26}$. The energy gap vs wave vector parallel to the a-b plane passing through the $Z = (0, 0, \pi)$ point. The presence of an isotropic gap at the center rules out d-wave superconductivity. From Xu *et al.*, 2012.

have nodes in that Z-centered pocket. Similar ARPES results were independently presented for $Tl_{0.63}K_{0.37}Fe_{1.78}Se_2$ (X.-P. Wang *et al.*, 2012). In this case the Z-centered electron FS has an isotropic SC gap ~6.2 meV. Both efforts conclude that d-wave superconductivity appears to be ruled out in these materials. However, the doping effects of Co on a pnictide (not a selenide) such as KFe_2As_2 have been interpreted via a d-wave SC state (A. F. Wang *et al.*, 2012), since the critical temperature rapidly decreases with increasing Co concentration, similarly as in cuprates. Thermal conductivity also suggests d-wave symmetry for the same material (Reid *et al.*, 2012).

Thus, if some pnictides appear to be d-wave superconductors, the symmetry of the SC state in the alkali metal iron selenides of focus here still needs to be further investigated.

How do all these ARPES results compare with similar pnictide investigations? The ARPES pnictides effort is large and will not be described here, but interested readers can consult Richard *et al.* (2011) for a recent review. In fact, there are many similarities between pnictides and selenides if it is simply accepted that the chemical potential for the case of Se is above the entire hole pocket band located at Γ. Thus, a transition occurs from a combination of hole and electron pockets for the pnictides to only electron pockets for the selenides.

These results are important for the FS nesting theories that may work for pnictides but not for selenides due to the absence of hole pockets. Thus, pairing mechanisms alternative to those based on weak-coupling spin-density-wave scenarios are needed for a proper description of the iron-based superconductors, such as purely electronic theories where the Hubbard coupling U is not small or theories where the lattice is involved in the Cooper-pair formation. Recent Lanczos investigations of the two-orbital Hubbard model in a broad range of Hubbard U and Hund J_H couplings and electronic density $n \sim 2$ (two electrons per Fe) concluded that s-wave pairing induced by magnetism is found not only at weak and intermediate couplings, but also at larger couplings where the parent compound becomes an insulator (Nicholson *et al.*, 2011) and there is no simple visual representation of the paired state based on a metallic FS. Then, while FS nesting may not be needed in the iron superconductors (Dai, Hu, and Dagotto, 2012) the pairing symmetry may still be s wave.

Returning to ARPES, the widely reported isotropic nature of the nodeless SC gaps is similar in both pnictides and selenides. However, in pnictides many bulk experiments suggest the presence of nodes in the SC state (Johnston, 2010; Stewart, 2011). Since ARPES is a surface-sensitive technique, the surface and the bulk could behave differently in these materials (Hirschfeld, Korshunov, and Mazin, 2011). Another important aspect to consider is that, for the special case of LiFeAs, recent ARPES experiments (Allan *et al.*, 2012; Umezawa *et al.*, 2012, and references therein) reported a moderate gap anisotropy along the FS, suggesting that complex anisotropic interactions are involved in the SC pairing, together with strong-coupling superconductivity since $2\Delta/k_BT_c$ can be larger than 6. Additional work is clearly needed to fully clarify the symmetry of the SC state for both pnictides and selenides.

VI. NEUTRON SCATTERING

Neutron scattering studies of the alkali metal iron selenides have revealed an unexpected and complex magnetic state in the presence of the ordered iron vacancies. The details are as follows.

A. Elastic neutron scattering

The first powder neutron diffraction studies of the alkali metal iron selenides were presented for $K_{0.8}Fe_{1.6}Se_2$ (Bao *et al.*, 2011), with Fe in a valence state $2+$. These investigations confirmed the presence of the $\sqrt{5}\times\sqrt{5}$ vacancy superstructure, compatible with results reviewed in Sec. II such as the single-crystal x-ray diffraction studies (Zavalij *et al.*, 2011). Other neutron diffraction studies of $Cs_yFe_{2-x}Se_2$, $A_xFe_{2-y}Se_2$ (A = Rb, K), and $Rb_yFe_{1.6+x}Se_2$ also concluded that there is a $\sqrt{5}\times\sqrt{5}$ iron-vacancy superstructure in the insulating state of these materials (Pomjakushin, Pomjakushina *et al.*, 2011; Pomjakushin, Sheptyakov *et al.*, 2011; Meng Wang *et al.*, 2011).

More importantly, Bao *et al.* (2011) reported a novel and exotic magnetic order in this compound that is stable in the iron-vacancy environment. This magnetic order contains 2×2 iron superblocks, with their four moments ferromagnetically aligned (see Fig. 12). These superblocks display an AFM order between them; thus the state will be referred to as the "block-AFM" state hereafter. The individual magnetic moments are $3.31\mu_B$/Fe, the largest observed in the family of iron-based superconductors. These neutron results, particularly the large magnetic moments, again challenge the view that these compounds are electronically weakly coupled and that FS nesting explains their behavior. While pnictides and selenides may have different Hubbard U coupling strengths, thus explaining their different properties, it could also occur that the view of the pnictides as weakly correlated materials is incorrect. More work is needed to clarify these matters. Adding to the discrepancy with the weak-coupling picture, an unprecedented high Néel temperature of

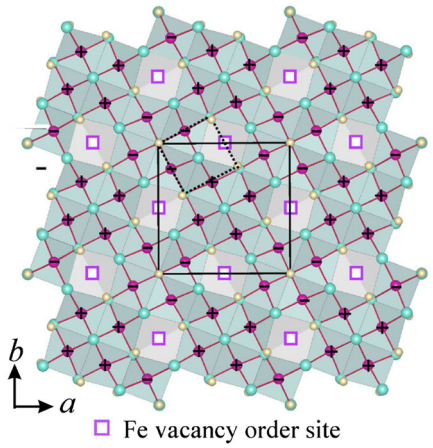

FIG. 12 (color online). In-plane crystal and magnetic structure of $K_{0.8}Fe_{1.6}Se_2$. The open squares are the iron vacancies and the dark circles with the "+" or "−" denote the occupied iron sites with the orientation of their spins. The open circles correspond to Se, while the K atoms are small open circles. From Bao *et al.*, 2011.

$T_N = 559$ K was reported for these iron-vacancy-ordered compounds. The magnetic ordering temperature is 20 K smaller than the order-disorder transition temperature for the iron vacancies.

Single-crystal neutron diffraction studies of $A_2Fe_4Se_5$ [A = Rb, Cs, (Tl,Rb), and (Tl,K)] by Ye *et al.* (2011) found the same iron-vacancy order and magnetic block-AFM states as observed in $K_2Fe_4Se_5$. The order-disorder transition occurs at $T_S = 500$–578 K, and the AFM transition at $T_N = 471$–559 K with a low-temperature magnetic moment $\sim 3.3\mu_B$/Fe. Ye *et al.* (2011) showed that all 245 iron selenides share a common crystalline and magnetic structure, which is very different from those of other iron-based superconductors such as the pnictides.

Neutron diffraction studies of $TlFe_{1.6}Se_2$ (Cao *et al.*, 2012; May *et al.*, 2012) unveiled spin arrangements that may deviate from the block-AFM order, compatible with theoretical calculations (Q. Luo *et al.*, 2011; Yin, Lin, and Ku, 2011; Yu, Goswami, and Si, 2011), where several spin states were found close in energy to the block-AFM state (see Sec. VII for details).

Moreover, neutron (Meng Wang *et al.*, 2011) and x-ray (Alessandro Ricci *et al.*, 2011) diffraction studies of the SC state also provided evidence for phase separation between the above-mentioned regular distribution of iron vacancies and another state with a $\sqrt{2} \times \sqrt{2}$ superstructure, as reported in other investigations reviewed in Sec. VII (theory). The important issue of phase separation was already discussed in Sec. III.

B. Inelastic neutron scattering

Inelastic neutron scattering studies (Miaoyin Wang *et al.*, 2011) showed that the spin waves of the insulating antiferromagnet $Rb_{0.89}Fe_{1.58}Se_2$, with the block-AFM order and Néel temperature of $\sim$500 K, can be accurately described by a local-moment Heisenberg model with iron nearest-neighbor (NN), next-NN (NNN), and next-NNN (NNNN) interactions, as reviewed by Dai, Hu, and Dagotto (2012). These results are in contrast to those for the iron pnictides, with As instead of Se, where contributions from itinerant electrons are needed to understand their spin-wave properties (Zhao *et al.*, 2009). Moreover, $Rb_{0.89}Fe_{1.58}Se_2$ has three spin-wave branches, while all other materials studied with neutrons have only one. However, as the energy of the spin excitations grows the neutron results of Miaoyin Wang *et al.* (2011) also show (see Fig. 13) an evolution from a low-energy state with eight peaks, as expected from the block-AFM state after averaging the two chiralities of the iron-vacancy distribution, to a high-energy state with spin waves very similar to those of pnictides such as $BaFe_2As_2$ in spite of their different Néel temperatures. This observation reveals intriguing common aspects in the magnetism of selenides and pnictides. In addition, a fitting analysis of the neutron spin-wave spectra shows that in these materials and others the effective NNN Heisenberg couplings (i.e., the coupling along the diagonal of an elementary iron plaquette) are all of similar value. Since in the same analysis the effective NN couplings (i.e., at the shortest Fe-Fe distance) vary more from material to material, even changing signs, the effective NNN coupling may be

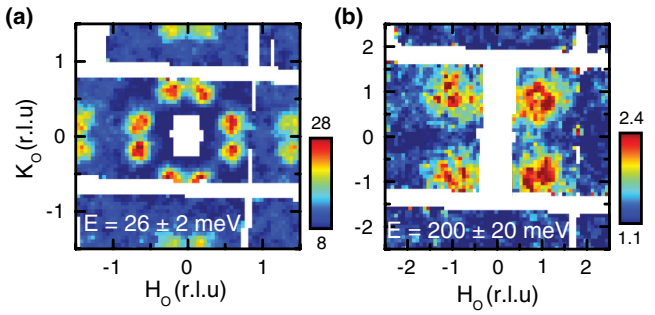

FIG. 13 (color online). Wave vector dependence of the spin-wave excitations of $Rb_{0.89}Fe_{1.58}Se_2$ at two representative energies (Miaoyin Wang *et al.*, 2011). (a) Eight peaks of the $\sqrt{5} \times \sqrt{5}$ iron distribution when the two chiralities are averaged; (b) is similar to results for $BaFe_2As_2$.

crucial to understanding the common properties of the iron-based superconductors (Miaoyin Wang *et al.*, 2011). In fact, a robust real (as opposed to effective) NNN superexchange coupling comparable to or larger in strength than the real NN superexchange is needed for the stability of the magnetic state with magnetic wave vector $(\pi, 0)$, in the iron-sublattice notation, that dominates in many iron-based superconductors. Recent results for superconducting $Rb_{0.82}Fe_{1.68}Se_2$ (Miaoyin Wang *et al.*, 2012) also suggest that the magnetic excitations arise from localized moments. For details see the recent review by Dai, Hu, and Dagotto (2012). Note that the spin-wave spectra have also been addressed using an *ab initio* linear response by Ke, Schilfgaarde, and Antropov (2012b).

Since its discovery in the context of the high-T_c Cu oxide superconductors, an aspect of the inelastic neutron scattering data that is considered of much importance is the neutron spin resonance (Scalapino, 2012). In superconducting $A_xFe_{2-y}Se_2$ the presence of neutron spin resonances was reported by Park *et al.* (2011), Friemel, Liu *et al.* (2012a), Friemel *et al.* (2012b), and Taylor *et al.* (2012) [see also Inosov *et al.* (2011)]. The energies of the resonances for many compounds are summarized in Fig. 14, showing that the normalized resonance energy is similar in all of the iron-based superconductors. The neutron results showing a resonance are

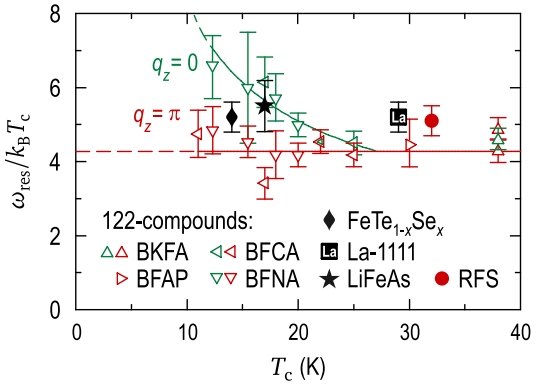

FIG. 14 (color online). Normalized resonance energy of several iron-based superconductors, from inelastic neutron scattering. RFS stands for $Rb_2Fe_4Se_5$, BFNA for $Ba(Fe_{1-x}Ni_x)_2As_2$, and the rest of the abbreviations are for 122, 111, or 1111 materials. From Park *et al.*, 2011.

compatible with the expectation arising from FS nesting involving the electron pockets for the case of a *d*-wave-symmetric condensate (Scalapino, 2012). However, the discussion is still open since FS nesting may not be sufficient to explain the properties of the iron-based superconductors, not even the pnictides (Dai, Hu, and Dagotto, 2012). Perhaps an intermediate Hubbard U coupling is a more appropriate starting point for the pnictides while the selenides may require an even stronger coupling. Also ARPES experiments reviewed in Sec. V tend to favor *s*-wave superconductivity due to the absence of nodes in the small electron pocket at Γ. Thus, the *d* vs *s* pairing symmetry of the alkali metal iron selenides remains an open and fascinating question.

VII. THEORY

A. Band structure in the presence of iron vacancies

The magnetic state of the alkali metal iron selenides has been investigated from the perspective of theory using a variety of techniques. For example, employing first-principles calculations and comparing several magnetic configurations, the ground state of $(K, Tl)_yFe_{1.6}Se_2$ was found to be the magnetic configuration with antiferromagnetically coupled 2×2 Fe blocks (Cao and Dai, 2011a), as reported in neutron scattering experiments. For $y = 0.8$ and K as the alkali element, a band gap ~600 meV opens, leading to an AFM insulator (Cao and Dai, 2011a). For $y = 1$, the Fermi level is near the top of the band gap of $y = 0.8$, leading to a metallic state with a ~400–550 meV gap slightly below the Fermi energy. Other *ab initio* calculations by Xun-Wang Yan *et al.* (2011) agree with these results, and band structure calculations for $K_xFe_2Se_2$ can also be found in Shein and Ivanovskii (2010) and Yan *et al.* (2011a). The block-AFM ground-state band structure is shown in Fig. 15. In addition, via studies of $K_{0.7}Fe_{1.6}Se_2$ and $K_{0.9}Fe_{1.6}Se_2$, i.e., varying the concentration of K to affect the valence of iron and the associated carrier concentration, it was found that the band structure and magnetic order almost do not change in that range of doping. Then $K_{0.8}Fe_{1.6}Se_2$ could be considered as a parent compound

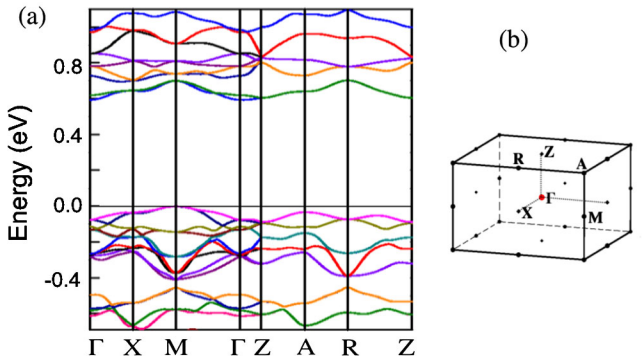

FIG. 15 (color online). (a) Electronic band structure of $K_{0.8}Fe_{1.6}Se_2$ in the ground state with the 2×2 block-AFM order. The top of the valence band is set to zero. (b) Explanation of the convention followed to label points of the Brillouin zone. These theoretical calculations are carried out in a tetragonal structure with lattice parameters in excellent agreement with experiments. From Xun-Wang Yan *et al.*, 2011.

which becomes superconducting upon electron or hole doping (Xun-Wang Yan *et al.*, 2011). This is relevant since in (Tl, K)Fe_xSe_2 superconductivity already occurs at $x = 1.7$ or higher (M. H. Fang *et al.*, 2011). However, the issue of phase separation discussed in Sec. III renders the identification of the parent compound far more complicated than naively anticipated.

B. Influence of electron-electron correlations

First-principles calculations for the related material $TlFe_{1.5}Se_2$ (i.e., with $Fe_{1.5}$ instead of $Fe_{1.6}$, and thus with a different distribution of iron vacancies) using the generalized gradient approximation (GGA) + U method were also reported by Cao and Dai (2011b). The conclusion is that the magnetic state, a spin-density wave, becomes stable because of an effective increase of U/W due to the reduction in the bandwidth W caused by the loss of electronic kinetic energy in a background with iron vacancies (Cao and Dai, 2011b; Chen, Cao, and Dai, 2011). This is similar to the conclusion of model calculations that addressed the stability of the block-AFM state for the case $Fe_{1.6}$ (Q. Luo *et al.*, 2011; Yin, Lin, and Ku, 2011; Yu, Zhu, and Si, 2011). In fact, the value $U \sim 2$ eV used by Cao and Dai (2011b) is similar to the $U \sim 3$ eV needed in the model Hamiltonian calculations (Q. Luo *et al.*, 2011) to stabilize the block-AFM spin state [for a recent experimental discussion on the U/W strength for the 1111 and 122 pnictides, see Vilmercati *et al.* (2012)]. The relevance of Mott physics, as opposed to an insulator caused by band structure effects, was also remarked by Craco, Laad, and Leoni (2011) using band structure plus dynamical mean-field theory. In fact, a more general study of the influence of correlations, not only in selenides but in pnictides as well, arrives at the conclusion that the weak-coupling Fermi surface nesting picture is incomplete and the intermediate-U coupling regime is more realistic (Yin, Haule, and Kotliar, 2011; Dai, Hu, and Dagotto, 2012).

Model calculations have been carried out using the multi-orbital Hubbard model. While using five orbitals offers the most realistic description of pnictides and selenides, the complexity of this many-body problem involving interacting electrons often requires a reduction in the number of orbitals to increase the accuracy of the calculations. Thus, one must often balance these two aspects. Using a three-orbital Hubbard model in the random-phase approximation (RPA), Huang and Mou (2011) also concluded that for $Fe_{1.6}$ the block-AFM spin state is caused by electron correlation effects, although at a smaller $U \sim 1.5$ eV than discussed previously. This is understandable since the three-orbital model requires a smaller U to represent the same physics as a five-orbital model (adjusting the electronic densities n for a proper comparison), due to the reduction in the bandwidths when reducing the number of orbitals. This value of U is also compatible with results by Luo *et al.* (2010) using a three-orbital model and electronic density per Fe orbital $n = 4/3$, but in the context of pnictides. Note that in the paper by Huang and Mou (2011) the ratio J_H/U is 0.2, similar to the 0.25 found by Q. Luo *et al.* (2011). Studies for pnictides also suggest a similar ratio for J_H/U (Luo *et al.*, 2010). Moreover, the importance of a robust J_H leading to a

so-called "Hund's metal" state has been remarked from the dynamical mean-field theory perspective (Georges, Medici, and Mravlje, 2013, and references therein) as well as from the orbital differentiation perspective [see Bascones, Valenzuela, and Calderón (2012), and references therein; for recent experimental results see Yi *et al.* (2013)], where some orbitals develop a gap with increasing U while others remain gapless, leading to a coexistence of localized and itinerant degrees of freedom. In addition, in the work by Q. Luo *et al.* (2011), and also via mean-field approximations and the three-orbital model by Lv, Lee, and Phillips (2011), it was concluded that for a sufficiently large U an orbitally ordered state should be stabilized for the iron-vacancies-ordered state, with the population of the d_{xz} and d_{yz} orbitals different at every iron site.

C. Competing states

The issue of the magnetic states that compete with the 2×2 block-AFM state [shown in Fig. 16(a)] has been addressed using a variety of techniques. Via first-principles calculations, the usual collinear AFM metallic phase [i.e., the phase with magnetic wave vector $(\pi, 0)$ with regard to the iron sublattice] was found to become stable if a pressure of 12 GPa is applied (Lei Chen *et al.*, 2011). This state corresponds to the same $(\pi, 0)$ magnetic order (C-AFM) as the 122 and 1111 families, simply removing the spins corresponding to the location of the iron vacancies [see Fig. 16(c)]. On further increasing the pressure to 25 GPa a nonmagnetic metallic state is reached (Lei Chen *et al.*, 2011). These results are qualitatively compatible with those found by Q. Luo *et al.* (2011) via Hartree-Fock (HF) approximations to the five-orbital Hubbard model at electronic density $n = 6$ (six electrons/Fe), since increasing pressure corresponds to increasing the hopping amplitudes in tight-binding Hamiltonians, thus increasing the carrier bandwidth W. Since the Hubbard U is local, it should not be affected by these effects as severely as W. Thus, a pressure increase amounts to a decrease in U/W in Hubbard model calculations. Indeed, working at a fixed $J_H/U = 0.25$, Q. Luo *et al.* (2011) found that reducing U/W at a constant J_H/U led to transitions from the block-AFM state [Fig. 16(a)] to the C-AFM state [Fig. 16(c)], and then eventually to a nonmagnetic state. If J_H/U is reduced, then the state shown in Fig. 16(b) could also be reached, with staggered order within the 2×2 blocks. The full HF phase diagram of the model is shown in Fig. 16(d). Also both the model and first-principles calculations agree on the reduction of the magnetic moment when moving from the block-AFM state to the C-AFM state.

As an alternative to the model Hamiltonian results, the first-principles calculations by Lei Chen *et al.* (2011) showed that the stabilization of the block-AFM state is caused by a lattice tetramer distortion; otherwise, the C-AFM state would be stable. This effect is not considered in the Hubbard model calculations where the block-AFM state is stabilized by an increase in U/W (Q. Luo *et al.*, 2011). Thus a combination of lattice distortions and electronic correlation effects may be needed to stabilize the block-AFM state in the presence of iron vacancies.

Note, however, that other first-principles simulations for $A_{0.8}Fe_{1.6}Se_2$ reported that pressure induces a transition from

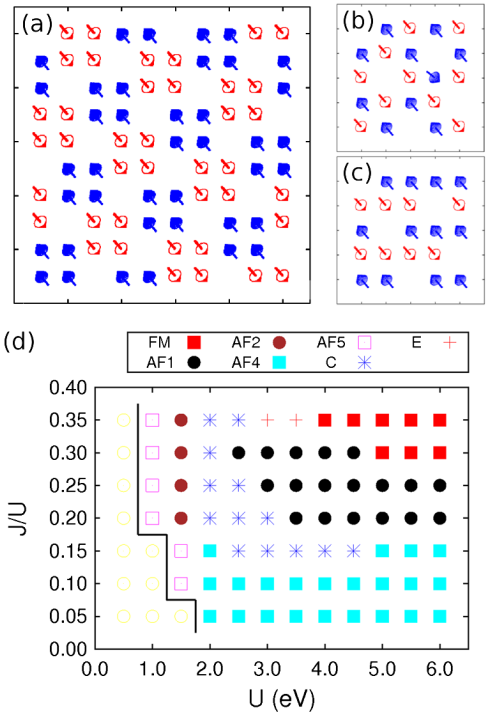

FIG. 16 (color online). (a)–(c) Some of the competing states in the presence of a $\sqrt{5} \times \sqrt{5}$ distribution of iron vacancies at $n = 6$. From Q. Luo *et al.*, 2011. (a) The experimentally dominant 2×2 block-AFM state, (b) a competing state found by Q. Luo *et al.* (2011) by reducing J_H/U, and (c) the C-type AFM state described by Lei Chen *et al.* (2011) and Q. Luo *et al.* (2011) that could be stabilized by increasing pressure. (d) Phase diagram of the five-orbital Hubbard model in the presence of the $\sqrt{5} \times \sqrt{5}$ iron-vacancy order, using Hartree-Fock (HF) techniques (Q. Luo *et al.*, 2011). A variety of phases are stable, including the state of (a) called "AF1" (often also called the plaquette state), the state of (b) called "AF4," and the state of (c) called "C." The FM phase is not shown because it is obvious, and for the remaining states "AF2," "AF5," and "E" see Cao and Dai (2011b), Q. Luo *et al.* (2011), and Yu, Goswami, and Si (2011).

the block-AFM state to the metallic "Néel-FM" state where each 2×2 block has staggered magnetic order (Cao, Fang, and Dai, 2011). The differences between these first-principles calculations are currently being jointly addressed by Cao, Fang, and Dai (2011) and Lei Chen *et al.* (2011) (C. Cao, private communication). As already remarked, note also that the model Hamiltonian calculations (Q. Luo *et al.*, 2011; Yin, Lin, and Ku, 2011) have unveiled several competing magnetic configurations that become stable in different regions of the J_H/U-U phase diagram [see Fig. 16(d)]; thus small variations in the first-principles calculations can lead to different states. These differences highlight the complexity of the phase diagram of various materials, displaying several competing phases when in the presence of iron vacancies. From the strong-coupling-limit perspective, calculations based on localized spin models for $A_{0.8}Fe_{1.6}Se_2$ also revealed many competing states, including the magnetic arrangement found in neutron experiments (Yu, Goswami, and Si, 2011; Fang *et al.*, 2012). A similar competition of states was found for $A_{0.8}Fe_{1.5}Se_2$, i.e., with $Fe_{1.5}$ instead of $Fe_{1.6}$ (Yu, Goswami, and Si, 2011). Note also that Li, Dong *et al.* (2012) predicted an insulating block-AFM spin state even

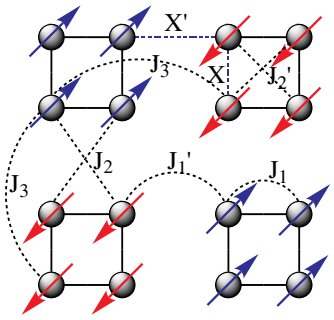

FIG. 17 (color online). The block-AFM spin order predicted for KFe_2Se_2 (no iron vacancies) based on spin model calculations. From Li, Dong *et al.*, 2012, where details can be found about the several Heisenberg couplings shown.

in the absence of iron vacancies, for instance, for KFe_2Se_2. This state is sketched in Fig. 17. The dominant magnetic instability of vacancies-free KFe_2Se_2 was also studied by Cao and Dai (2011c), reporting a state similar to that of pnictides and a FS with only electronlike pockets without nesting, and by Da-Yong Liu *et al.* (2012).

D. Pairing symmetry

As discussed, the states with chemical composition $A_{0.8}Fe_{1.6}Se_2$, $AFe_{1.5}Se_2$, and AFe_2Se_2 have received considerable attention both experimentally and theoretically. Predicting the pairing symmetry of the SC state in these materials has been one of the areas of focus. Using a slave-spin technique to study the Mott transition of a two-orbital Hubbard model, and an effective perturbation theory once the system is in the Mott state, the superconductivity of slightly doped $(Tl, K)Fe_{1.5}Se_2$ was studied, unveiling a competition regulated by J_H between a d-wave state (with a positive order parameter in two of the electronlike pockets and negative in the other two) and an s-wave state with the same sign of the order parameter in the electron pockets (there are no hole pockets in these materials) (Yi Zhou *et al.*, 2011). The importance of superconductivity mediated by spin fluctuations was also analyzed using spin-fermion models, i.e., mixing itinerant and localized degrees of freedom as opposed to directly using a Hubbard model (Zhang, Lu, and Xiang, 2011). For $K_xFe_{2-y}Se_2$, the fluctuation exchange approximation applied to a five-orbital Hubbard model (Maier *et al.*, 2011) leads to d-wave superconductivity due to pair scattering between the electron pockets. The RPA enhanced static susceptibility has a broad peak at (π, π) in the Fe sublattice notation. A similar d-wave pairing was found using the two-orbital model within the RPA (Das and Balatsky, 2011), and a possible $s + id$ pairing was also discussed by Rong Yu *et al.* (2011). The results of Maier *et al.* (2011) contain a robust dependence of the SC gap with a wave vector along the electron pockets.

However, ARPES results seem to be in disagreement with d-wave pairing (X.-P. Wang *et al.*, 2012; Xu *et al.*, 2012). In addition, the calculations that lead to d-wave superconductivity have been criticized because they are based on the "unfolded" Brillouin zone (BZ), neglecting the symmetry lowering of the staggered Se atom positions (Mazin, 2011). Based on this consideration, Mazin (2011) argued that the d-wave states should develop nodal lines at the folded BZ electron pockets, which are not observed experimentally. It was then concluded that either a conventional same-sign s-wave state, with the same sign for the SC order parameter in all the FS pockets, or another form of the s_{+-} state, different from the one proposed for the pnictides, should be the dominant symmetry [(Mazin, 2011; You *et al.*, 2011); for details and references on the possible pairing channels discussed in the literature, see Johnston (2010); for another form of s_{+-} pairing for AFe_2Se_2, see Khodas and Chubukov (2012)]. The dominance of s-wave pairing was also concluded from mean-field studies based on magnetic exchange couplings (Chen Fang *et al.*, 2011). They remarked that s-wave pairing can exist even without the electron and hole pockets needed in weak coupling. Lanczos calculations by Nicholson *et al.* (2011) reached similar conclusions. The d-wave versus s-wave competition, the latter with the same sign in all pockets, was also studied by Saito, Onari, and Kontani (2011) via orbital and spin fluctuations in models for KFe_2Se_2. For the orbital fluctuations a small electron-phonon coupling is needed. In the phase-separation context, the differences between d-wave and s-wave pairing for the superconducting proximity effect in the magnetic state and the suppression of the magnetic moments were also addressed via two-orbital models and mean-field approximations [see Jiang *et al.* (2012); a related work to test the pairing symmetry via nonmagnetic impurities was proposed by Wang, Yao, and Zhang (2013)].

E. Other topics addressed by theory

Several other topics have been addressed using theoretical techniques. For example, (i) the effect of disordered vacancies on the electronic structure of $K_xFe_{2-y}Se_2$ was studied using new Wannier function methods (Berlijn, Hirschfeld, and Ku, 2012) and also via the two-orbital Hubbard model in the mean-field approximation (Tai *et al.*, 2012). Also in this context and to distinguish between the d-wave and s-wave pairing channels in the absence of hole pockets, it was argued that the influence of nonmagnetic impurity scattering needs to be considered (Zhu and Bishop, 2011). Similar issues were addressed by Zhu *et al.* (2011). In addition, it has been argued that adding Fe atoms to $K_2Fe_{4+x}Se_5$ creates impurity bands that have common features with iron pnictides, thus addressing the coexistence of superconductivity and magnetic states (Ke, Schilfgaarde, and Antropov, 2012a). (ii) Band structure calculations have shown that the stoichiometric KFe_2Se_2 has a rather different FS than Ba122, but still the d_{xz}, d_{yz}, and d_{xy} orbitals dominate at the Fermi energy (Nekrasov and Sadovskii, 2011).

VIII. TWO-LEG LADDERS

A. Introduction and experiments

Considering the vast interest in the alkali metal iron selenides summarized in the previous sections, and also considering that deviations from an iron square lattice, as in the presence of iron-vacancy order, lead to interesting physics, other crystal geometries are worth exploring. In this section, recent experimental efforts (Caron *et al.*, 2011; Krzton-Maziopa, Pomjakushina *et al.*, 2011; Lei, Ryu, Frenkel,

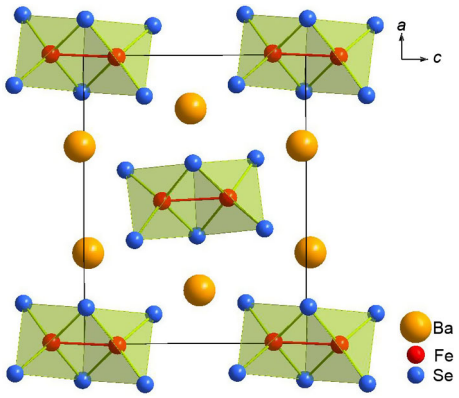

FIG. 18 (color online). The two-leg ladder substructures of $BaFe_2Se_3$, with their legs oriented perpendicular to the figure. From Lei, Ryu, Frenkel, and Petrovic, 2011.

and Petrovic, 2011; Saparov *et al.*, 2011; Caron *et al.*, 2012; Nambu *et al.*, 2012) in the study of selenides with the geometry of two-leg ladders (sometimes also referred to as double chains) are reviewed. A typical compound in this context is $BaFe_2Se_3$ containing building blocks made of $[Fe_2Se_3]^{2-}$ that when assembled along a particular direction lead to an array of two-leg ladder structures, as sketched in Fig. 18.

The ladders in $BaFe_2Se_3$ can be considered as cutouts of the layers of edge-sharing $FeSe_4$ tetrahedra of the two-dimensional selenides (see Fig. 19). Each ladder has a long direction ("legs") and a short direction involving two Fe atoms ("rungs"). A field of research involving similar ladder structures, but with spin-1/2 copper instead of iron, is also very active since in that context two interesting effects were found: a spin gap and superconductivity upon doping (Dagotto, Riera, and Scalapino, 1992; Dagotto and Rice, 1996). For instance, $SrCu_2O_3$ is a material analogous to $BaFe_2Se_3$ (Dagotto, 1999).

$BaFe_2Se_3$ is an insulator with a gap 0.14–0.18 eV (Lei, Ryu, Frenkel, and Petrovic, 2011; Nambu *et al.*, 2012). This material has long-range AFM order at ~250 K, low-temperature magnetic moments $\sim 2.8\mu_B$, and short-range AFM order (presumably along the leg directions) at higher temperatures (Caron *et al.*, 2011; Lei, Ryu, Frenkel, and Petrovic, 2011; Saparov *et al.*, 2011). Establishing an interesting analogy with the alkali metal iron selenides, neutron

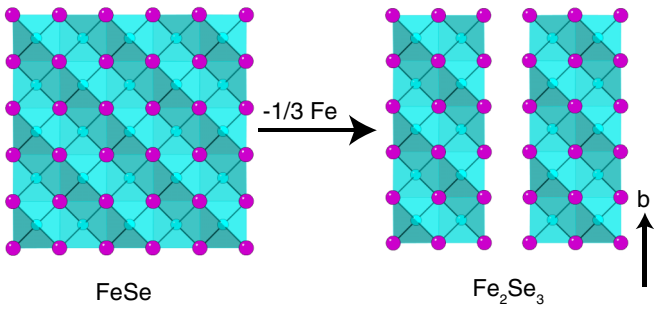

FIG. 19 (color online). Relation between a complete FeSe layer and the structure of the ladders. The dark spheres are the Se atoms and the light spheres are the Fe atoms. The ladders simply amount to the removal of every third iron atom from the layers. From Saparov *et al.*, 2011.

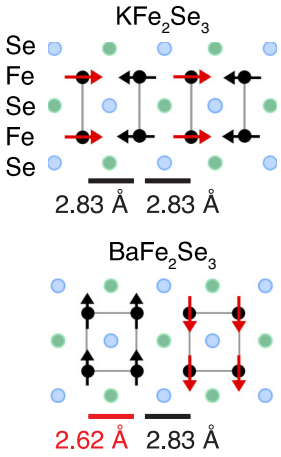

FIG. 20 (color online). Magnetic order of the two-leg ladders for the cases of KFe_2Se_3 and $BaFe_2Se_3$ obtained using neutron diffraction. From Caron *et al.*, 2012.

diffraction studies (Caron *et al.*, 2011; Nambu *et al.*, 2012) reported a dominant order involving 2×2 blocks of ferromagnetically aligned iron spins, with these blocks antiferromagnetically ordered, as shown in Fig. 20 (lower panel). These building blocks are the same as in the block-AFM state of the $\sqrt{5} \times \sqrt{5}$ iron-vacancy arrangement. Thus, understanding one case may lead to progress in the other. When the Ba atoms of $BaFe_2Se_3$ are replaced by K, eventually arriving at KFe_2Se_3, the magnetic order changes to that in Fig. 20 (upper panel), with spins along the rungs coupled ferromagnetically, and with an AFM coupling along the legs (Caron *et al.*, 2012).

B. Theory

The theoretical study of selenide ladders is only at an early stage. First-principles calculations and spin model studies (W. Li, Setty *et al.*, 2012) showed the dominance of the block-AFM state found experimentally. The band structure calculation in this magnetic state was presented by W. Li, Setty *et al.* (2012) [see also Saparov *et al.* (2011)] and it contains a gap of 0.24 eV (see Fig. 21).

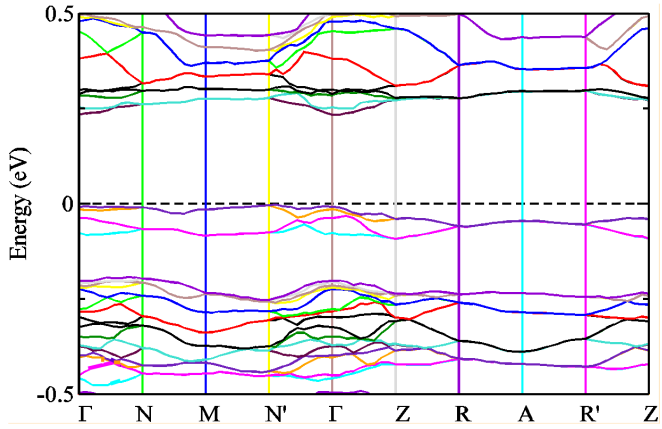

FIG. 21 (color online). Electronic band structure of the block-AFM state of the two-leg ladder $BaFe_2Se_3$. The gap is 0.24 eV. From W. Li, Setty *et al.*, 2012.

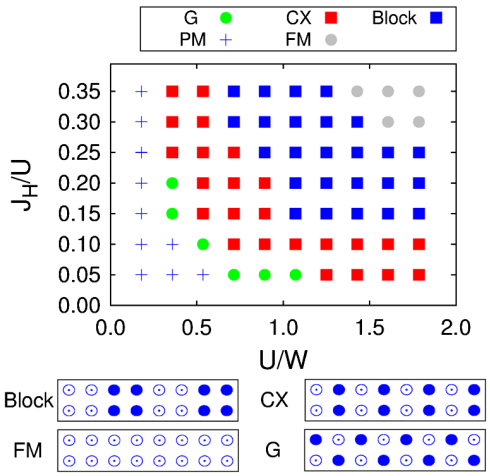

FIG. 22 (color online). Phase diagram of the five-orbital Hubbard model in the real-space HF approximation, at electronic density $n = 5.75$ (n is the number of electrons per iron), using a 2×16 lattice. J_H in units of U and U in units of the bandwidth W are varied. PM stands for paramagnetic and FM for ferromagnetic. The other magnetic states are schematically shown at the bottom. The hoppings used are from band structure calculations corresponding to $BaFe_2Se_3$. From Luo *et al.*, 2013.

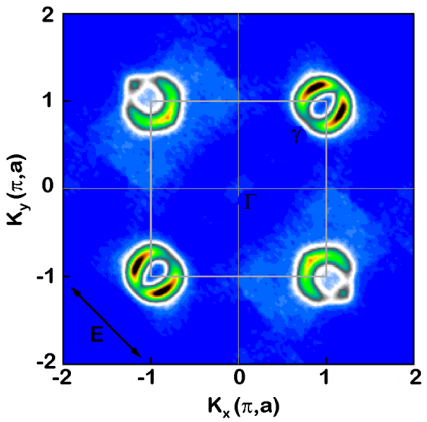

FIG. 23 (color online). Fermi surface of a single-layer FeSe superconductor using ARPES techniques. Only electronlike pockets are present. From Defa Liu *et al.*, 2012.

With regard to model Hamiltonians, calculations using the five-orbital Hubbard model in the HF approximation have been reported by Luo *et al.* (2013). By varying U and J_H, the phase diagram in Fig. 22 was found. The block-AFM phase ("block" in the figure) is stable in a robust portion of the phase diagram. This includes the regime with the ratio $J_H/U = 0.25$ widely believed to be realistic for these compounds. Moreover, the other phase of ladders that was recently reported in neutron experiments (Caron *et al.*, 2012), denoted as CX in the figure, is also part of the phase diagram. In addition, other phases not yet observed experimentally are also stable on varying the couplings, suggesting that many states are close in energy and likely competing. Figure 22 (lower panel) contains a sketch of the relevant states. Note also that the ratio U/W starts at ~ 0.6 for the block phase, indicating again that these materials are in the intermediate-coupling regime, instead of weak or strong coupling. Results for a two-orbital model are compatible with those found via the five-orbital model (Luo *et al.*, 2013).

Our understanding of ladder iron selenides is still primitive and more work should be carried out in this context. The main advantage of studying ladders is that the quasi-one-dimensionality of these systems allows for more accurate theoretical calculations than those routinely performed for two-dimensional systems, thus improving the back-and-forth iterative process between theory and experiments needed to understand these materials.

IX. RELATED AND RECENT DEVELOPMENTS

An exciting recent result is the report of superconductivity in a single-unit-cell FeSe film grown on $SrTiO_3$ (Q.-Y. Wang *et al.*, 2012), displaying signatures of the SC transition above 50 K, and a SC gap as large as 20 meV. The electronic structure of this single-layer FeSe superconductor was studied via ARPES techniques by Defa Liu *et al.* (2012). The FS is shown in Fig. 23 and it consists only of electron pockets near the zone corner, without any indication of even a small pocket at the zone center. This is contrary to the band structure calculations reported in the same publication that predicted a pocket at Γ. Thus, there are no scattering channels between the Γ and M points of the Brillouin zone. The top of the holelike band at Γ is 80 meV below the Fermi level. The critical temperature is ~55 K and the SC gap was found to be large and nearly isotropic, and since this is a strictly two-dimensional system, the presence of nodes along the z axis is ruled out. From first-principles calculations Liu, Lu, and Xiang (2012) concluded that the single- and double-layer FeSe films are weakly doped AFM semiconductors, i.e., for the monolayer FeSe to be superconducting doped electrons may be needed via O or Se vacancies. Clearly, the in-depth study of this single-layer system contributes significantly to the understanding of the SC state of the iron superconductors.

While completing this Colloquium two new results were reported: (1) the SC T_c of the single-layer FeSe film grown on a $SrTiO_3$ substrate was optimized to $T_c = 65 \pm 5$ K via an annealing process (He *et al.*, 2012), establishing a new T_c record for the iron superconductors. Photoemission studies indicate a FS with electron pockets at the M points (He *et al.*, 2012), as in the previous report by Defa Liu *et al.* (2012). (2) A single layer of alkali-metal-doped FeSe with the geometry of weakly coupled two-leg ladders was prepared by Wei Li *et al.* (2012c) and shown to become superconducting based on the presence of a gap in the local DOS. This suggests that the pairing is likely local and establishes analogies with the Cu oxide ladders (Dagotto and Rice, 1996).

There are several other exciting recent topics of research in these materials. As discussed, the insulating characteristics of some of the alkali metal iron selenides suggests that Mott physics may be important for understanding their properties. For instance, the iron oxychalcogenides $La_2O_2Fe_2O(Se, S)_2$ were studied theoretically, and the conclusion is that they are Mott insulators because of enhanced correlation effects caused by band narrowing (Zhu *et al.*, 2010). The importance of Mott localization was also addressed for $K_{0.8}Fe_{1.7}S_2$ and $K_{0.8}Fe_{1.7}SeS$ (Guo *et al.*, 2011), and also for $BaFe_2Se_2O$ (Han *et al.*, 2012; Lei *et al.*, 2012). Lei, Abeykoon,

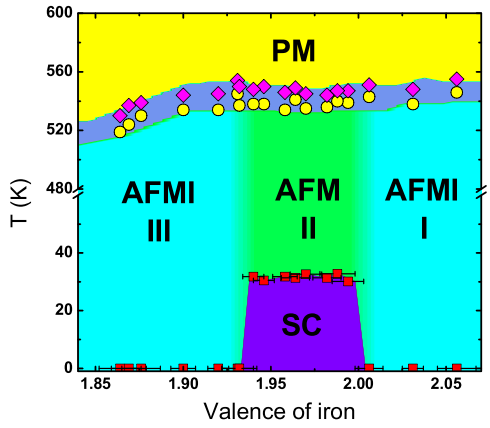

FIG. 24 (color online). The phase diagram of $K_xFe_{2-y}Se_2$ vs the iron valence. The SC phase appears sandwiched between AFM insulators. The Fe valence state was systematically controlled by varying the x and y concentrations in $K_xFe_{2-y}Se_2$. From Yan *et al.*, 2012.

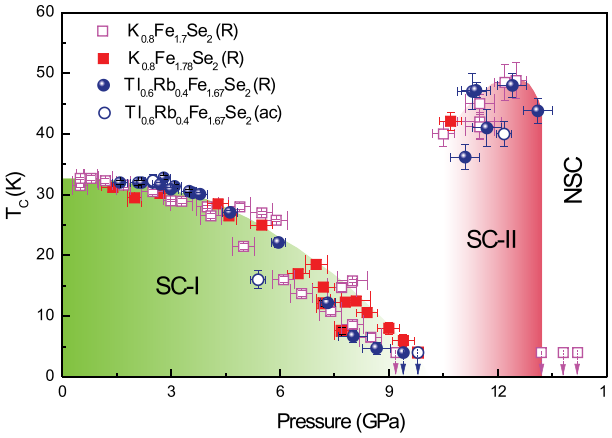

FIG. 25 (color online). Superconducting T_c vs pressure for the compounds indicated. Two SC phases were found. SC-II has a $T_c \sim 48.7$ K. From Sun *et al.*, 2012.

Bozin, Wang *et al.* (2011) studied the phase diagram of $K_xFe_{2-y}Se_{2-z}S_z$, showing that T_c is suppressed as the S concentration increases [see also Lei, Abeykoon, Bozin, and Petrovic (2011) and Lei, Bozin *et al.* (2011)].

In a related context, the $K_{0.8}Fe_{2-x}Co_xSe_2$ phase diagram was discussed by T. T. Zhou *et al.* (2011). A small amount of Co suppresses the superconductivity of the undoped material, and at $x = 0.03$ there is no longer a zero-resistivity state. They argued that this behavior is similar to that of Cu oxide superconductors and for this reason the alkali metal iron selenides are better described by localized $3d$ spins than by itinerant electrons.

Also among the most recent developments is the study of the phase diagram of $A_xFe_{2-y}Se_2$ (A = K, Rb, and Cs) versus the valence of iron (Yan *et al.*, 2012). This iron valence was controlled by systematically varying x and y. The resulting phase diagram is shown in Fig. 24 and it contains three AFM insulating states (characterized by different iron-vacancy superstructures) and a SC state. Since the SC phase is surrounded by insulators, Yan *et al.* (2012) concluded that the SC phase must have those insulating states as parent compounds.

Another interesting result is the discovery of a second "reemerging" SC phase (Sun *et al.*, 2012) for $Tl_{0.6}Rb_{0.4}Fe_{1.67}Se_2$, $K_{0.8}Fe_{1.7}Se_2$, and $K_{0.8}Fe_{1.78}Se_2$, with critical temperatures $T_c \sim 48$–49 K, when the pressure is increased to 11.5 GPa (see Fig. 25). The changes of T_c with increasing pressure may be caused by structural variances within the basic tetragonal unit cell, and the $\sqrt{5} \times \sqrt{5}$ iron-vacancy order may be destroyed by pressure-driving the system into a disordered lattice. The possibility of a novel quantum critical point in this material was also discussed by Guo *et al.* (2012).

Along similar lines with regard to increases in T_c, superconductivity at 30–46 K in $A_xFe_2Se_2$ using small-size alkali metals and alkaline earth atoms (A = Li, Na, Ba, Sr, Ca, Yb, and Eu) was recently observed by Ying *et al.* (2012). Compatible with these results, superconductivity at 44 K in $A_xFe_{2-y}Se_2$ was also recently reported (Zhang, Xia *et al.*, 2013). At these temperatures a sharp drop in resistivity and susceptibility was observed. The 44 K SC phase is close to an ideal 122 structure, but with an unexpectedly large c-axis lattice parameter 18.10 Å: Zhang, Xia *et al.* (2013) showed a plot that T_c increases with the distance between neighboring FeSe layers. Related to these results, superconductivity at 43 K in $Li_x(NH_2)_y(NH_3)_{1-y}Fe_2Se_2$ ($x = 0.6$; $y = 0.2$) (Burrard-Lucas *et al.*, 2012), at 44 K in $Li_xFe_2Se_2(NH_3)_y$ (Scheidt *et al.*, 2012), and at 45 K in $Li_x(C_5H_5N)_yFe_{2-z}Se_2$ (Krzton-Maziopa *et al.*, 2012) was also recently observed.

X. CONCLUSIONS

In this Colloquium the "hot" topic of alkali metal iron selenides was reviewed. The main reasons for the current excitement in this area of research include the realization that these materials do not have hole pockets at the Γ point, conceptually altering the dominant perception that originated in the pnictides about the importance of FS nesting between electron and hole pockets to understand the magnetic and SC states. This conclusion is compatible with the recent accumulation of evidence that FS nesting and a weak-coupling perspective are not sufficient for the pnictides (Dai, Hu, and Dagotto, 2012). Moreover, via ARPES techniques applied to some alkali metal iron selenides, the small electron (not hole) pocket at Γ was investigated and in the SC state this pocket does not present nodes, removing the d-wave state as a possibility (although this issue is still under discussion). Thus, the menu of options for the symmetry of the SC order parameter in these selenides appears reduced to a conventional same-sign s-wave state (via a coupling of the electrons to the lattice), or a more exotic form of the s_{+-} state (Mazin, 2011), different from the s_{+-} state proposed for the pnictides (Johnston, 2010). Also note that the same-sign s wave may not explain the neutron spin resonances in the alkali metal iron selenides (Scalapino, 2012). Thus, only further work can clarify this subtle matter.

Another reason for the excitement in this area of research is the possibility of having an insulating parent compound of the SC state, perhaps a Mott insulator. Candidate states with an ordered distribution of iron vacancies have been identified at particular compositions of iron. Some of these states display an exotic magnetic state that contains 2×2 blocks of aligned iron moments, with an AFM coupling between

blocks. Other states have also been proposed as parent compounds, and a final answer has not been given to this matter.

In this same context of exploring Mott insulators in the iron-superconductor arena, note that iron has been replaced by other transition metal elements, such as Mn, leading to interesting results including AFM insulators and metallic states upon doping, although not yet to superconductivity. For the case of $BaMn_2As_2$, see Johnston *et al.* (2011) and Pandey *et al.* (2012), and references therein. This line of exploration is promising and it should be further pursued.

Finally, the presence of phase separation has also attracted considerable attention. Are the magnetic and SC states competing or cooperating? This is also a recurrent open question for the SC copper oxides as well. Note that such competition or cooperation is relevant only if the states can influence one another either by sharing the same volume element, i.e., microscopically coexisting, or by forming an inhomogeneous state at such short length scales that one state can still affect the other and vice versa. In fact, in several FeAs-based materials there is evidence that the two competing states share the same volume element (Johnston, 2010), while in the selenides the situation is still evolving with regard to the length scales involved in the phase-separation process.

In summary, the young subfield of alkali metal iron selenides is challenging the prevailing ideas for the pnictides. It might be that selenides and pnictides harbor different pairing mechanisms, or they may have different strengths in their Hubbard U couplings. After all, the pnictides have AFM metallic states as parent compounds of superconductivity, while the selenides may have AFM insulators as parent compounds, based on the discussion presented here. However, by arguments of simplicity it is also reasonable to assume that a unique qualitative mechanism could be at work simultaneously in both families of compounds. Perhaps short-range AFM fluctuations may be similarly operative as the pairing mechanism in the context of both metallic and insulating parent states. All these important issues are still under much discussion, and by focusing on the new alkali metal iron selenides several intriguing conceptual questions raised by the discovery of the iron-based superconductors may soon converge in an answer.

ACKNOWLEDGMENTS

The author thanks D. C. Johnston and A. Moreo for a careful reading of this manuscript and for making valuable suggestions to improve the quality of the presentation. The author also thanks W. Bao, A. Bianconi, A. V. Boris, M. J. Calderón, Chao Cao, A. Charnukha, Xi Chen, Xialong Chen, Xianhui Chen, Jianhui Dai, Pengcheng Dai, Hong Ding, Shuai Dong, M. H. Fang, D. L. Feng, P. J. Hirschfeld, C. Homes, J. P. Hu, D. S. Inosov, B. Keimer, Z.-Y. Lu, Qinlong Luo, T. A. Maier, G. Martins, T. M. McQueen, Tian Qian, C. Petrovic, A. Ricci, A. Safa-Sefat, D. J. Scalapino, Gang Wang, Miaoyin Wang, Tao Xiang, Q. K. Xue, Yajun Yan, Feng Ye, Rong Yu, H. Q. Yuan, Fuchun Zhang, and X. J. Zhou for many useful comments. The author is supported by the U.S. DOE, Office of Basic Energy Sciences, Materials Sciences and Engineering Division, and by the National Science Foundation under Grant No. DMR-1104386.

REFERENCES

Allan, M. P., A. W. Rost, A. P. Mackenzie, Yang Xie, J. C. Davis, K. Kihou, C. H. Lee, A. Iyo, H. Eisaki, and T.-M. Chuang, 2012, Science **336**, 563.

Bao, W., Q. Huang, G. F. Chen, M. A. Green, D. M. Wang, J. B. He, X. Q. Wang, and Y. Qiu, 2011, Chin. Phys. Lett. **28**, 086104.

Bao, Wei, G. N. Li, Q. Huang, G. F. Chen, J. B. He, M. A. Green, Y. Qiu, D. M. Wang, and J. L. Luo, 2013, Chin. Phys. Lett. **30**, 027402.

Bascones, E., B. Valenzuela, and M. J. Calderón, 2012, Phys. Rev. B **86**, 174508.

Berlijn, Tom, P. J. Hirschfeld, and Wei Ku, 2012, arXiv:1204.2849.

Borisenko, S. V., *et al.*, 2012, arXiv:1204.1316.

Bosak, A., V. Svitlyk, A. Krzton-Maziopa, E. Pomjakushina, K. Conder, V. Pomjakushin, A. Popov, D. de Sanctis, and D. Chernyshov, 2011, arXiv:1112.2569.

Burrard-Lucas, M. *et al.*, 2012, arXiv:1203.5046.

Cai, Peng, Cun Ye, Wei Ruan, Xiaodong Zhou, Aifeng Wang, Meng Zhang, Xianhui Chen, and Yayu Wang, 2012, Phys. Rev. B **85**, 094512.

Cao, Chao, and Jianhui Dai, 2011a, Phys. Rev. Lett. **107**, 056401.

Cao, Chao, and Jianhui Dai, 2011b, Phys. Rev. B **83**, 193104.

Cao, Chao, and Jianhui Dai, 2011c, Chin. Phys. Lett. **28**, 057402.

Cao, Chao, Minghu Fang, and Jianhui Dai, 2011, arXiv:1108.4322.

Cao, H., C. Cantoni, A. F. May, M. A. McGuire, B. C. Chakoumakos, S. J. Pennycook, R. Custelcean, A. S. Sefat, and B. C. Sales, 2012, Phys. Rev. B **85**, 054515.

Caron, J. M., J. R. Neilson, D. C. Miller, K. Arpino, A. Llobet, and T. M. McQueen, 2012, Phys. Rev. B **85**, 180405(R).

Caron, J. M., J. R. Neilson, D. C. Miller, A. Llobet, and T. M. McQueen, 2011, Phys. Rev. B **84**, 180409(R).

Charnukha, A., *et al.*, 2012a, Phys. Rev. Lett. **109**, 017003.

Charnukha, A., *et al.*, 2012b, Phys. Rev. B **85**, 100504(R).

Chen, F., *et al.*, 2011, Phys. Rev. X **1**, 021020.

Chen, Hua, Chao Cao, and Jianhui Dai, 2011, Phys. Rev. B **83**, 180413.

Chen, Lei, Xun-Wang Yan, Zhong-Yi Lu, and Tao Xiang, 2011, arXiv:1109.3049.

Chen, Z. G., R. H. Yuan, T. Dong, G. Xu, Y. G. Shi, P. Zheng, J. L. Luo, J. G. Guo, X. L. Chen, and N. L. Wang, 2011, Phys. Rev. B **83**, 220507(R).

Craco, L., M. S. Laad, and S. Leoni, 2011, Phys. Rev. B **84**, 224520.

Dagotto, E., 1994, Rev. Mod. Phys. **66**, 763.

Dagotto, E., 1999, Rep. Prog. Phys. **62**, 1525.

Dagotto, E., and T. M. Rice, 1996, Science **271**, 618.

Dagotto, E., J. A. Riera, and D. J. Scalapino, 1992, Phys. Rev. B **45**, 5744.

Dai, Pengcheng, Jiangping Hu, and Elbio Dagotto, 2012, Nat. Phys. **8**, 709.

Das, Tanmoy, and A. V. Balatsky, 2011, Phys. Rev. B **84**, 014521.

Das, Tanmoy, Anton B. Vorontsov, Ilya Vekhter, and Matthias J. Graf, 2012, Phys. Rev. Lett. **109**, 187006.

Fang, C., B. Xu, P. Dai, T. Xiang, and J. P. Hu, 2012, Phys. Rev. B **85**, 134406.

Fang, Chen, Yang-Le Wu, Ronny Thomale, B. Andrei Bernevig, and Jiangping Hu, 2011, Phys. Rev. X **1**, 011009.

Fang, M. H., H. M. Pham, B. Qian, T. J. Liu, E. K. Vehstedt, Y. Liu, L. Spinu, and Z. Q. Mao, 2008, Phys. Rev. B **78**, 224503.

Fang, M. H., H. D. Wang, C. H. Dong, Z. J. Li, C. M. Feng, J. Chen, and H. Q. Yuan, 2011, Europhys. Lett. **94**, 27 009.

Friemel, G., W. P. Liu, E. A. Goremychkin, Y. Liu, J. T. Park, O. Sobolev, C. T. Lin, B. Keimer, D. S. Inosov, 2012a, Europhys. Lett. **99**, 67004.
Friemel, G., *et al.* 2012b, Phys. Rev. B **85**, 140511(R).
Garbarino, G., R. Weht, A. Sow, A. Sulpice, P. Toulemonde, M. Álvarez-Murga, P. Strobel, P. Bouvier, M. Mezouar, and M. Núez-Regueiro, 2011, Phys. Rev. B **84**, 024510.
Georges, Antoine, Luca de' Medici, and Jernej Mravlje, 2013, Annu. Rev. Condens. Matter Phys. **4**, 137, and references therein.
Guo, J., S. Jin, G. Wang, S. Wang, K. Zhu, T. Zhou, M. He, and X. L. Chen, 2010, Phys. Rev. B **82**, 180520(R).
Guo, J. G., X. L. Chen, G. Wang, T. T. Zhou, X. F. Lai, S. F. Jin, S. C. Wang, and K. X. Zhu, 2011, arXiv:1102.3505.
Guo, Jing, *et al.*, 2012, Phys. Rev. Lett. **108**, 197001.
Han, Fei, Xiangang Wan, Bing Shen, and Hai-Hu Wen, 2012, arXiv:1206.6154.
He, Shaolong, *et al.*, 2012, arXiv:1207.6823.
Hirschfeld, P. J., M. M. Korshunov, and I. I. Mazin, 2011, Rep. Prog. Phys. **74**, 124508.
Homes, C. C., Z. J. Xu, J. S. Wen, and G. D. Gu, 2012a, Phys. Rev. B **85**, 180510(R).
Homes, C. C., Z. J. Xu, J. S. Wen, and G. D. Gu, 2012b, arXiv:1208.2240.
Hsu, F. C., *et al.*, 2008, Proc. Natl. Acad. Sci. U.S.A. **105**, 14 262.
Huang, Shin-Ming, and Chung-Yu Mou, 2011, Phys. Rev. B **84**, 184521.
Inosov, D. S., J. T. Park, A. Charnukha, Yuan Li, A. V. Boris, B. Keimer, and V. Hinkov, 2011, Phys. Rev. B **83**, 214520.
Jiang, Hong-Min, Wei-Qiang Chen, Zi-Jian Yao, and Fu-Chun Zhang, 2012, Phys. Rev. B **85**, 104506.
Johnston, D. C., 2010, Adv. Phys. **59**, 803.
Johnston, D. C., R. J. McQueeney, B. Lake, A. Honecker, M. E. Zhitomirsky, R. Nath, Y. Furukawa, V. P. Antropov, and Yogesh Singh, 2011, Phys. Rev. B **84**, 094445, and references therein.
Julien, M.-H., H. Mayaffre, M. Horvati, C. Berthier, X. D. Zhang, W. Wu, G. F. Chen, N. L. Wang, and J. L. Luo, 2009, Europhys. Lett. **87**, 37 001.
Kamihara, Y., T. Watanabe, M. Hirano, and H. Hosono, 2008, J. Am. Chem. Soc. **130**, 3296.
Ke, Liqin, Mark van Schilfgaarde, and Vladimir Antropov, 2012a, Solid State Commun. **152**, 1846.
Ke, Liqin, Mark van Schilfgaarde, and Vladimir Antropov, 2012b, Phys. Rev. B **86**, 020402(R).
Khodas, M., and A. V. Chubukov, 2012, Phys. Rev. Lett. **108**, 247003.
Kotegawa, H., Y. Hara, H. Nohara, H. Tou, Y. Mizuguchi, H. Takeya, and Y. Takano, 2011, J. Phys. Soc. Jpn. **80**, 043708.
Kotegawa, H., Y. Tomita, H. Tou, Y. Mizuguchi, H. Takeya, and Y. Takano, 2012, arXiv:1206.1756.
Krzton-Maziopa, A., E. Pomjakushina, V. Pomjakushin, D. Sheptyakov, D. Chernyshov, V. Svitlyk, and K. Conder, 2011, J. Phys. Condens. Matter **23**, 402201.
Krzton-Maziopa, A., E. V. Pomjakushina, V. Yu. Pomjakushin, F. von Rohr, A. Schilling, and K. Conder, 2012, arXiv:1206.7022.
Krzton-Maziopa, A., Z. Shermadini, E. Pomjakushina, V. Pomjakushin, M. Bendele, A. Amato, R. Khasanov, H. Luetkens, and K. Conder, 2011, J. Phys. Condens. Matter **23**, 052203.
Ksenofontov, V., G. Wortmann, S. A. Medvedev, V. Tsurkan, J. Deisenhofer, A. Loidl, and C. Felser, 2011, Phys. Rev. B **84**, 180508(R).
Lazarević, N., M. Abeykoon, P. W. Stephens, Hechang Lei, E. S. Bozin, C. Petrovic, and Z. V. Popović, 2012, Phys. Rev. B **86**, 054503.
Lei, H., H. Ryu, A. I. Frenkel, and C. Petrovic, 2011, Phys. Rev. B **84**, 214511.
Lei, Hechang, Milinda Abeykoon, Emil S. Bozin, and C. Petrovic, 2011, Phys. Rev. B **83**, 180503(R).
Lei, Hechang, Milinda Abeykoon, Emil S. Bozin, Kefeng Wang, J. B. Warren, and C. Petrovic, 2011, Phys. Rev. Lett. **107**, 137002.
Lei, Hechang, Emil S. Bozin, Kefeng Wang, and C. Petrovic, 2011, Phys. Rev. B **84**, 060506(R).
Lei, Hechang, Hyejin Ryu, John Warren, A. I. Frenkel, V. Ivanovski, B. Cekic, and C. Petrovic, 2012, arXiv:1206.5788.
Li, J. Q., Y. J. Song, H. X. Yang, Z. Wang, H. L. Shi, G. F. Chen, Z. W. Wang, Z. Chen, and H. F. Tian, 2011, arXiv:1104.5340.
Li, W., C. Setty, X. H. Chen, and J. P. Hu, 2012, arXiv:1202.4016.
Li, Wei, Shuai Dong, Chen Fang, and Jiangping Hu, 2012, Phys. Rev. B **85**, 100407(R).
Li, Wei, *et al.*, 2012a, Nat. Phys. **8**, 126.
Li, Wei, *et al.*, 2012b, Phys. Rev. Lett. **109**, 057003.
Li, Wei, *et al.*, 2012c, arXiv:1210.4619.
Liu, Da-Yong, Ya-Min Quan, Zhi Zeng, and Liang-Jian Zou, 2012, Physica (Amsterdam) **407B**, 1139.
Liu, Defa *et al.*, 2012, Nat. Commun. **3**, 931.
Liu, K., Z. Y. Lu, and T. Xiang, 2012, Phys. Rev. B **85**, 235123.
Liu, R. H., *et al.*, 2011, Europhys. Lett. **94**, 27 008.
Liu, Y., Z. C. Li, W. P. Liu, G. Friemel, D. S. Inosov, R. E. Dinnebier, Z. J. Li, and C. T. Lin, 2012, Supercond. Sci. Technol. **25**, 075001.
Luo, Q., A. Nicholson, J. Riera, D.-X. Yao, A. Moreo, and E. Dagotto, 2011, Phys. Rev. B **84**, 140506(R).
Luo, Q. L., G. Martins, D.-X. Yao, M. Daghofer, R. Yu, A. Moreo, and E. Dagotto, 2010, Phys. Rev. B **82**, 104508.
Luo, Q. L., A. Nicholson, J. Rincón, S. Liang, J. Riera, G. Alvarez, L. Wang, W. Ku, G. Samolyuk, A. Moreo, and E. Dagotto, 2013, Phys. Rev. B **87**, 024404.
Luo, X. G., *et al.*, 2011, New J. Phys. **13**, 053011.
Lv, Weicheng, Wei-Cheng Lee, and Philip Phillips, 2011, Phys. Rev. B **84**, 155107.
Ma, Long, G. F. Ji, J. Zhang, J. B. He, D. M. Wang, G. F. Chen, Wei Bao, and Weiqiang Yu, 2011, Phys. Rev. B **83**, 174510.
Maier, T. A., S. Graser, P. J. Hirschfeld, and D. J. Scalapino, 2011, Phys. Rev. B **83**, 100515(R).
Margadonna, S., Y. Takabayashi, Y. Ohishi, Y. Mizuguchi, Y. Takano, T. Kagayama, T. Nakagawa, M. Takata, and K. Prassides, 2009, Phys. Rev. B **80**, 064506.
May, A. F., M. A. McGuire, H. Cao, I. Sergueev, C. Cantoni, B. C. Chakoumakos, D. S. Parker, and B. C. Sales, 2012, Phys. Rev. Lett. **109**, 077003.
Mazin, I. I., 2011, Phys. Rev. B **84**, 024529.
Mizuguchi, Y., Y. Hara, K. Deguchi, S. Tsuda, T. Yamaguchi, K. Takeda, H. Kotegawa, H. Tou, and Y. Takano, 2010, Supercond. Sci. Technol. **23**, 054013.
Mizuguchi, Y., H. Takeya, Y. Kawasaki, T. Ozaki, S. Tsuda, T. Yamaguchi, and Y. Takano, 2011, Appl. Phys. Lett. **98**, 042511.
Mou, D. X., *et al.*, 2011, Phys. Rev. Lett. **106**, 107001.
Mou, Daixiang, Lin Zhao, and Xingjiang Zhou, 2011, Front. Phys. **6**, 410.
Nambu, Y., *et al.*, 2012, Phys. Rev. B **85**, 064413;
Nekrasov, I. A., and M. V. Sadovskii, 2011, JETP Lett. **93**, 166.
Nicholson, A., W. H. Ge, X. Zhang, J. A. Riera, M. Daghofer, A. M. Oleś, G. B. Martins, A. Moreo, and E. Dagotto, 2011, Phys. Rev. Lett. **106**, 217002.
Paglione, J., and R. L. Greene, 2010, Nat. Phys. **6**, 645.
Pandey, Abhishek, *et al.*., 2012, Phys. Rev. Lett. **108**, 087005, and references therein.

Park, J. T., *et al.*, 2011, Phys. Rev. Lett. **107**, 177005.
Pomjakushin, V. Yu., E. V. Pomjakushina, A. Krzton-Maziopa, K. Conder, D. Chernyshov, V. Svitlyk, and A. Bosak, 2012, J. Phys. Condens. Matter **24**, 435701.
Pomjakushin, V. Yu., E. V. Pomjakushina, A. Krzton-Maziopa, K. Conder, and Z. Shermadini, 2011, J. Phys. Condens. Matter **23**, 156003.
Pomjakushin, V. Yu., D. V. Sheptyakov, E. V. Pomjakushina, A. Krzton-Maziopa, K. Conder, D. Chernyshov, V. Svitlyk, and Z. Shermadini, 2011, Phys. Rev. B **83**, 144410.
Qian, T., *et al.*, 2011, Phys. Rev. Lett. **106**, 187001.
Qiu, Y., *et al.*, 2008, Phys. Rev. Lett. **101**, 257002.
Reid, J.-Ph. *et al.*, 2012, Supercond. Sci. Technol. **25**, 084013.
Ren, Z., *et al.*, 2008, Europhys. Lett. **83**, 17002.
Ricci, A., *et al.*, 2011, Phys. Rev. B **84**, 060511(R).
Ricci, Alessandro, *et al.*, 2011, Supercond. Sci. Technol. **24**, 082002.
Richard, P., T. Sato, K. Nakayama, T. Takahashi, and H. Ding, 2011, Rep. Prog. Phys. **74**, 124512.
Ryan, D. H., W. N. Rowan-Weetaluktuk, J. M. Cadogan, R. Hu, W. E. Straszheim, S. L. Bud'ko, and P. C. Canfield, 2011, Phys. Rev. B **83**, 104526.
Saito, Tetsuro, Seiichiro Onari, and Hiroshi Kontani, 2011, Phys. Rev. B **83**, 140512(R).
Saparov, B., S. Calder, B. Sipos, H. Cao, S. Chi, D. J. Singh, A. D. Christianson, M. D. Lumsden, and A. S. Sefat, 2011, Phys. Rev. B **84**, 245132.
Scalapino, D. J., 1995, Phys. Rep. **250**, 329.
Scalapino, D. J., 2012, arXiv:1207.4093 [Rev. Mod. Phys. (to be published)].
Scheidt, E.-W., V. R. Hathwar, D. Schmitz, A. Dunbar, W. Scherer, V. Tsurkan, J. Deisenhofer, and A. Loidl, 2012, arXiv:1205.5731.
Shein, I. R., and A. L. Ivanovskii, 2010, arXiv:1012.5164, and references therein.
Shen, B., B. Zeng, G. F. Chen, J. B. He, D. M. Wang, H. Yang, and H. H. Wen, 2011, Europhys. Lett. **96**, 37010.
Shermadini, Z., H. Luetkens, R. Khasanov, A. Krzton-Maziopa, K. Conder, E. Pomjakushina, H.-H. Klauss, and A. Amato, 2012, Phys. Rev. B **85**, 100501(R).
Shermadini, Z., *et al.*, 2011, Phys. Rev. Lett. **106**, 117602.
Simonelli, L., N. L. Saini, M. Moretti Sala, Y. Mizuguchi, Y. Takano, H. Takeya, T. Mizokawa, and G. Monaco, 2012, Phys. Rev. B **85**, 224510.
Song, Y. J., Z. Wang, Z. W. Wang, H. L. Shi, Z. Chen, H. F. Tian, G. F. Chen, H. X. Yang, and J. Q. Li, 2011, arXiv:1104.4844.
Stewart, G. R., 2011, Rev. Mod. Phys. **83**, 1589.
Sun, Liling, *et al.*, 2012, Nature (London) **483**, 67.
Tai, Yuan-Yen, Jian-Xin Zhu, Matthias J. Graf, and C. S. Ting, 2012, Phys. Rev. B **86**, 134512.
Tamai, A., *et al.*, 2010, Phys. Rev. Lett. **104**, 097002.
Taylor, A. E., R. A. Ewings, T. G. Perring, J. S. White, P. Babkevich, A. Krzton-Maziopa, E. Pomjakushina, K. Conder, A. T. Boothroyd, 2012, Phys. Rev. B **86**, 094528.
Texier, Y., J. Deisenhofer, V. Tsurkan, A. Loidl, D. S. Inosov, G. Friemel, and J. Bobroff, 2012, Phys. Rev. Lett. **108**, 237002.
Torchetti, D. A., M. Fu, D. C. Christensen, K. J. Nelson, T. Imai, H. C. Lei, and C. Petrovic, 2011, Phys. Rev. B **83**, 104508.
Umezawa, K., *et al.*, 2012, Phys. Rev. Lett. **108**, 037002.
Vilmercati, P., *et al.*, 2012, Phys. Rev. B **85**, 235133.
Wang, A. F., *et al.*, 2011, Phys. Rev. B **83**, 060512(R).
Wang, A. F., *et al.*, 2012, arXiv:1206.2030.
Wang, C. N., *et al.*, 2012, Phys. Rev. B **85**, 214503.
Wang, D. M., J. B. He, T.-L. Xia, and G. F. Chen, 2011, Phys. Rev. B **83**, 132502.
Wang, F., and D. H. Lee, 2011, Science **332**, 200.
Wang, Hangdong, Chihen Dong, Zujuan Li, Shasha Zhu, Qianhui Mao, Chunmu Feng, H. Q. Yuan, and Minghu Fang, 2011, Europhys. Lett. **93**, 47004.
Wang, Kefeng, Hechang Lei, and C. Petrovic, 2011a, Phys. Rev. B **83**, 174503.
Wang, Kefeng, Hechang Lei, and C. Petrovic, 2011b, Phys. Rev. B **84**, 054526.
Wang, Meng *et al.*, 2011, Phys. Rev. B **84**, 094504.
Wang, Miaoyin, Chunhong Li, D. L. Abernathy, Yu Song, Scott V. Carr, Xingye Lu, Shiliang Li, Zahra Yamani, Jiangping Hu, Tao Xiang, and Pengcheng Dai, 2012, Phys. Rev. B **86**, 024502.
Wang, Miaoyin, *et al.*, 2011, Nat. Commun. **2**, 580.
Wang, Q.-Y., *et al.*, 2012, Chin. Phys. Lett. **29**, 037402.
Wang, Qian-En, Zi-Jian Yao, and Fu-Chun Zhang, 2013, Europhys. Lett. **101**, 57002.
Wang, X.-P., T. Qian, P. Richard, P. Zhang, J. Dong, H.-D. Wang, C.-H. Dong, M.-H. Fang, and H. Ding, 2011, Europhys. Lett. **93**, 57001.
Wang, X.-P., *et al.*, 2012, Europhys. Lett. **99**, 67 001.
Wang, Z., Y. J. Song, H. L. Shi, Z. W. Wang, Z. Chen, H. F. Tian, G. F. Chen, J. G. Guo, H. X. Yang, and J. Q. Li, 2011, Phys. Rev. B **83**, 140505(R).
Wang, Z. W., Z. Wang, Y. J. Song, C. Ma, H. L. Shi, Z. Chen, H. F. Tian, H. X. Yang, G. F. Chen, and J. Q. Li, 2012, J. Phys. Chem. C **116**, 17847.
Xu, M., *et al.*, 2012, Phys. Rev. B **85**, 220504(R).
Yan, X.-W., M. Gao, Z. Y. Lu, and T. Xiang, 2011a, Phys. Rev. B **84**, 054502.
Yan, X.-W., M. Gao, Z.-Y. Lu, and T. Xiang, 2011b, Phys. Rev. Lett. **106**, 087005.
Yan, Xun-Wang, Miao Gao, Zhong-Yi Lu, and Tao Xiang, 2011, Phys. Rev. B **83**, 233205.
Yan, Y. J., M. Zhang, A. F. Wang, J. J. Ying, Z. Y. Li, W. Qin, X. G. Luo, J. Q. Li, Jiangping Hu, and X. H. Chen, 2012, Sci. Rep. **2**, 212.
Ye, F., S. Chi, Wei Bao, X. F. Wang, J. J. Ying, X. H. Chen, H. D. Wang, C. H. Dong, and M. H. Fang, 2011, Phys. Rev. Lett. **107**, 137003.
Yeh, K. W., *et al.*, 2008, Europhys. Lett. **84**, 37002.
Yi, M. *et al.*, 2013, Phys. Rev. Lett. **110**, 067003.
Yin, Wei-Guo, Chia-Hui Lin, and Wei Ku, 2011, arXiv:1106.0881, and references therein.
Yin, Z. P., K. Haule, and G. Kotliar, 2011, Nat. Mater. **10**, 932.
Ying, J. J., *et al.*, 2011, Phys. Rev. B **83**, 212502.
Ying, T. P., X. L. Chen, G. Wang, S. F. Jin, T. T. Zhou, X. F. Lai, H. Zhang, and W. Y. Wang, 2012, Sci. Rep. **2**, 426.
You, Yi-Zhuang, Fan Yang, Su-Peng Kou, and Zheng-Yu Weng, 2011, Phys. Rev. Lett. **107**, 167001.
Yu, Rong, Pallab Goswami, and Qimiao Si, 2011, Phys. Rev. B **84**, 094451.
Yu, Rong, Pallab Goswami, Qimiao Si, Predrag Nikolic, and Jian-Xin Zhu, 2011, arXiv:1103.3259.
Yu, Rong, Jian-Xin Zhu, and Qimiao Si, 2011, Phys. Rev. Lett. **106**, 186401.
Yu, Weiqiang, L. Ma, J. B. He, D. M. Wang, T.-L. Xia, G. F. Chen, and Wei Bao, 2011, Phys. Rev. Lett. **106**, 197001.
Yuan, R. H., T. Dong, Y. J. Song, P. Zheng, G. F. Chen, J. P. Hu, J. Q. Li, and N. L. Wang, 2012, Sci. Rep. **2**, 221.
Zavalij, P., *et al.*, 2011, Phys. Rev. B **83**, 132509.
Zeng, B., B. Shen, G. F. Chen, J. B. He, D. M. Wang, C. H. Li, and H. H. Wen, 2011, Phys. Rev. B **83**, 144511.

Zhang, A. M., K. Liu, J. H. Xiao, J. B. He, D. M. Wang, G. F. Chen, B. Normand, and Q. M. Zhang, 2012, Phys. Rev. B **85**, 024518.
Zhang, A. M., T. L. Xia, K. Liu, W. Tong, Z. R. Yang, and Q. M. Zhang, 2013, Sci. Rep. **3**, 1216.
Zhang, A. M., J. H. Xiao, Y. S. Li, J. B. He, D. M. Wang, G. F. Chen, B. Normand, Q. M. Zhang, and T. Xiang, 2012, Phys. Rev. B **85**, 214508 (2012).
Zhang, G. M., Z. Y. Lu, and T. Xiang, 2011, Phys. Rev. B **84**, 052502, and references therein.
Zhang, Y., *et al.*, 2011, Nat. Mater. **10**, 273.
Zhao, J., D. T. Adroja, D.-X. Yao, R. Bewley, S. L. Li, X. F. Wang, G. Wu, X. H. Chen, J. P. Hu, and P. Dai, 2009, Nat. Phys. **5**, 555.
Zhao, Jun, Huibo Cao, E. Bourret-Courchesne, D.-H. Lee, and R. J. Birgeneau, 2012, Phys. Rev. Lett. **109**, 267003.
Zhao, Lin, *et al.*, 2011, Phys. Rev. B **83**, 140508(R).
Zhou, T. T., X. L. Chen, J. G. Guo, G. Wang, X. F. Lai, S. C. Wang, S. F. Jin, and K. X. Zhu, 2011, arXiv:1102.3506.
Zhou, Yi, Dong-Hui Xu, Fu-Chun Zhang, and Wei-Qiang Chen, 2011, Europhys. Lett. **95**, 17 003.
Zhu, J.-X., R. Yu, H. D. Wang, L. L. Zhao, M. D. Jones, J. H. Dai, E. Abrahams, E. Morosan, M. H. Fang, and Q. Si, 2010, Phys. Rev. Lett. **104**, 216405.
Zhu, Jian-Xin, and A. R. Bishop, 2011, arXiv:1109.4162.
Zhu, Jian-Xin, Rong Yu, A. V. Balatsky, and Qimiao Si, 2011, Phys. Rev. Lett. **107**, 167002.